Supplementary information for

Horizontally Oriented Pyrido[2,3-*b*]pyrazine-Based Thermally Activated Delayed Fluorescence Emitters Exhibiting Bipolar Charge Transport for Efficient Organic Light-Emitting Diodes

Domantas Lekavičius[1], Rasa Keruckiene[1], Matas Guzauskas[1], Dmytro Volyniuk[1], Juozas V. Grazulevicius[1*]

[1]*Department of Polymer Chemistry and Technology, Kaunas University of Technology, K. Barsausko St. 59, LT-50254, Kaunas, Lithuania*

Table of contents

Instrumentation **2**

Materials **4**

Synthesis **4**

Figures **8**

Optimisation of OLEDs **28**

Tables **32**

References **33**

[*]Corresponding authors: Rasa Keruckiene: rasa.keruckiene@ktu.lt; Juozas V. Grazulevicius juozas.grazulevicius@ktu.lt

Instrumentation

The mass spectra of the compounds were recorded on a *Waters SQ Detector 2* spectrometer. The data obtained are presented as mass-to-charge ratio (m/z) versus signal strength (%).

IR spectra were recorded using a *Vertex 70 Bruker* spectrometer. The analysis was performed using the attenuated total reflection (ATR) method. Spectral data are presented as a function of wave number (v) versus transmittance (T).

Nuclear magnetic resonance spectra of ^{1}H (400 MHz) and ^{13}C (101 MHz) were recorded on a *Bruker Avance III* spectrometer. The spectral data is reported in parts per million (ppm). Samples were prepared by dissolving 10 mg of the tested substance in 0.7 ml of deuterated chloroform ($CDCl_3$).

Cyclic voltammetry measurements were made with an *Autolab III* potentiostat/galvanostat. The electrochemical cell used consisted of 3 electrodes (Pt/silicon as working electrode, Pt as auxiliary electrode and Ag as reference electrode). The measurements were carried out for the solutions in dry dichloromethane containing 0.1 M tetrabutylammonium hexafluorophosphate at 25 °C; the scan rate was 50 mV/s, the sample concentration was 10^{-3} M. The potentials were calibrated with the standard ferrocene/ferrocenium (Fc/Fc^{+}) redox system.

Thermogravimetric analysis (TGA) was carried out using a *TA Instruments Q50 analyser*. The samples were heated at 20 °C/min. to 800 °C.

Differential scanning calorimetry (DSC) measurements were performed on a *TA Instruments DSC Q2000* system. Samples were heated and cooled at a rate of 10 °C/min.

UV/Vis absorption spectra of the compounds' toluene dilute (10^{-4}-10^{-5} M) solutions and thin films were recorded under ambient conditions on a *Perkin Elmer Lambda 35* spectrometer. Fluorescence spectra of the compounds' toluene dilute (10^{-4}-10^{-5} M) solutions, pure, Zeonex and other thin films were recorded at room temperature on an *Edinburgh Intstruments FLS 980* fluorometer. PL quantum yields of the solutions and thin films were measured using an integrating sphere.

Ionisation potentials of thin films were determined by photoelectron emission spectroscopy. The thin-films were prepared by casting the material dissolved in chloroform on a clean substrate. A negative voltage of 300 V was applied to the sample substrate. A UV deuterium light source *ASBN*-

D130-CM and a *CM110 1/8 m* monochromator were used to illuminate the samples with monochromatic light.

Charge transporting properties of vacuum-deposited films of pyrido[2,3-*b*]pyrazines were studied by the time-of-flight (TOF) method at room temperature [5]. The sample configuration was indium tin oxide (ITO) /organic layer/Al. The thicknesses (*d*) of the layers were measured by ProFilm3D profilometer (**Figure S18**). A laser (EKSPLA) with a wavelength of 355 nm, the precision 6517B electrometer (Keithley), and the TDS 3032C oscilloscope (Tektronix) were used in the TOF setup. The samples were excited by the laser from the ITO side. Positive voltages (*V*) were applied to ITO to record hole carrier transients with visible transit times (t_{tr}) at the different electric fields (*E*). Hole mobilities (μ_h) of compounds were calculated using the formula $\mu_h = d^2 / (V \times t_{tr})$. The electric field dependence of the hole and electron mobility values were in good agreement with the following Poole–Frenkel formula: $\mu = \mu_0 \exp \beta E^{1/2}$.

The formula includes zero field mobility (μ_0), and the electric field dependence (β), which is related to the slopes of the fitting curves. The relatively high values of β result from dispersive hole and electron transport of compounds **3**-**6** (Table 3). Since holes and electrons traverse the films at the different times, the plateau and tail regions of the TOF curves are not observable on the plots with the linear scales.

All density functional theory (DFT) and time-dependent DFT (TD-DFT) calculations were performed using the PBE0 hybrid functional [1] with the def2-SVP basis set [2], as implemented in the Gaussian 16 software [3]. To gain insight into the nature and spatial characteristics of the electronic excitations, natural transition orbitals were generated for both the first singlet and first triplet excited states.

Thin films for emission quantum efficiency, ionisation potential, charge transport and ADPL measurements were prepared by vacuum deposition using an *MB EcoVap4G* system under inert atmosphere. The base pressure was $\leq 2 \times 10^{-6}$ Pa, and the deposition rate was maintained at 0.5–1.5 Å/s.

Film thickness and surface roughness were measured using a *ProFilm3D* optical profilometer by analyzing reflected light and height variations.

Angle-dependent photoluminescence (ADPL) measurements were performed using a *Fluxim Phelos* system to evaluate the molecular orientation in thin films. The samples were optically coupled to a glass prism using a SPI Supplies Series A Cargille Refractive Index Matching Fluid (ND=1.516) to ensure efficient light transmission. Photoluminescence spectra were recorded as a function of the emission angle relative to the surface.

OLEDs were fabricated by vacuum deposition using an *MB EcoVap4G* system under inert atmosphere. The base pressure was $\leq 2 \times 10^{-6}$ Pa, and the deposition rate was maintained at 0.5–1.5 Å/s depending on the layer. Doped devices were fabricated by controlling the deposition rates of the host and guest in separate crucibles. Layers of PEDOT:PSS were prepared by spin coating. Current density–voltage–luminance (*J–V–L*) characteristics were recorded using a *Keithley 6517* electrometer immediately after device fabrication. Luminance was measured with a calibrated *PH100-Si-HA-D0* photodiode. Current efficiency (cd/A), power efficiency (lm/W), and external quantum efficiency (EQE, %) were calculated from the *J–V–L* and EL data. Electroluminescence spectra were recorded on an *Avaspec-2048L* spectrometer.

Materials

2-(4-Bromophenyl)-2-oxoacetaldehyde was purchased from AmBeed and used as received. 2,3-Diaminopyridine, 4,4'-dibromobenzil, ferrocene, and sodium tert-butoxide were purchased from Aldrich and used as received. Phenothiazine and carbazole were purchased from Sigma–Aldrich and used as received. Tris(dibenzylideneacetone)dipalladium(0) and XPhos were purchased from Fluorochem and used as received. Tetrabutylammonium hexafluorophosphate was purchased from Labochema and used as received. Acetone, chloroform, dichloromethane, ethyl acetate, hexane, methanol, and toluene were purchased from Eurochemicals. All were used as received, except toluene, which was distilled before use.

Synthesis

3-(4-Bromophenyl)pyrido[2,3-*b*]pyrazine (PP-Br). 1.5 g (1 equiv.) 2,3-diaminopyridine, 2.93 g (1 equiv.) 2-(4-bromophenyl)-2-oxoacetaldehyde and 40 ml glacial acetic acid were placed in a round-bottomed flask with a magnetic stirrer. An air condenser was attached to the flash which was then heated on an electric hotplate. The reaction is carried out at boiling point for 24 hours. After this time, the mixture is cooled and poured into a beaker with ice water. The resulting mixture is put into a separating funnel and the organic phase is extracted using chloroform. After extraction,

the material obtained is recrystallised from methanol. A light brown powder (3.184 g, 80.9 %) is obtained. MM = 286.13 g/mol, **$C_{13}H_8BrN_3$**.

^{1}H NMR (400 MHz, $CDCl_3$) δ: 9.42 (s, **1H**), 9.19 (d, J = 2.7 Hz, **1H**), 8.48 (d, J = 8.6 Hz, **1H**), 8.22 (d, J = 8.1 Hz, **2H**), 7.72 (d, J = 8.3 Hz, **3H**).

^{13}C NMR (101 MHz, $CDCl_3$) δ: 155, 154, 151, 144, 138, 137, 135, 133, 130, 126, 125.

2,3-Bis(4-bromophenyl)pyrido[2,3-*b*]pyrazine (PP-2Br). 0.561 g (1 equiv.) 2,3-diamino pyridine, 1.89 g (1 eq.) 4,4'-dibromobenzil and 30 ml of glacial acetic acid were placed in a round-bottomed flash with a magnetic stirret. The reaction and purification of the substance is carried out in analogy with that of compound **1**. A dark brown powder (0.753 g, 34 %) is obtained. MM = 441.13 g/mol, **$C_{19}H_{11}Br_2N_3$**.

^{1}H NMR (400 MHz, $CDCl_3$) δ: 9.19 (dd, J = 4.2; 1.9 Hz, **1H**), 8.51 (d, J = 8.4 Hz, **1H**), 7.75 (dd, J = 8.5; 4.2 Hz, **1H**), 7.57 – 7.49 (m, **6H**), 7.44 (d, J = 8.5 Hz, **2H**).

^{13}C NMR (101 MHz, $CDCl_3$) δ: 154, 154, 153, 149, 138, 137, 136, 136, 132, 132, 131, 131, 131, 131, 125, 124, 124.

9-(4-(Pyrido[2,3-*b*]pyrazin-3-yl)phenyl)-9*H*-carbazole (3). 0.9 g (1 equiv.) of **PP-Br**, 1.05 g (2 equiv.) of carbazole, 1.06 g (3.5 equiv.) of sodium tert-butoxide, 0.144 g (0.05 equiv.) of tris(dibenzylideneacetone)dipalladium(0), 0.075 g (0.05 equiv.) of the ligand XPhos (2-(2-(dicyclohexylphosphine)-2',4',6'-tri-isopropyl-1,1'-biphenyl) and 20 ml of dry degassed toluene was added to a Schlenk flask with a magnetic stirrer. The flask was purged with nitrogen gass and then heated on an electric hotplate. The reaction is then carried out at boiling point for 24 hours. After the reaction, the mixture is cooled and the product purified by column chromatography. Hexane, a mixture of hexane and ethyl acetate (4:1, 3:1, 2:1, 1:1) is used as the eluent. A light yellowish powder (0.576 g, 49 %) is obtained. MM = 372.43 g/mol, **$C_{25}H_{16}N_4$**.

MS: m/z: 372 [M^+].

^{1}H NMR (400 MHz, $CDCl_3$) δ: 9.57 (s, **1H**), 9.24 (d, J = 2.7 Hz, **1H**), 8.61 (d, J = 8.2 Hz, **2H**), 8.53 (d, J = 8.3 Hz, **1H**), 8.17 (d, J = 7.7 Hz, **2H**), 7.84 (d, J = 8.1 Hz, **2H**), 7.75 (dd, J = 8.4; 4.2 Hz, **1H**), 7.54 (d, J = 8.2 Hz, **2H**), 7.46 (t, J = 7.7 Hz, **2H**), 7.33 (t, J = 7.4 Hz, **2H**).

^{13}C NMR (101 MHz, $CDCl_3$) δ: 154, 153, 151, 144, 140, 140, 138, 137, 134, 129, 127, 126, 125, 123, 120, 109.

10-(4-(Pyrido[2,3-*b*]pyrazin-3-yl)phenyl)-10*H*-phenothiazine (4). 0.504 g (1 equiv.) of **PP-Br**, 0.702 g (2 equiv.) of 10*H*-phenothiazine, 0.592 g (3.5 equiv.) of sodium tert-butoxide, 0.081 g (0.05 equiv.) of tris(dibenzylideneacetone)dipalladium(0), 0.042 g (0.05 equiv.) of the ligand XPhos (2-(2-(dicyclohexylphosphine)-2',4',6'-tri-isopropyl-1,1'-biphenyl) and 15 ml of dry degassed toluene was added to a Schlenk flask with magnetic stirrer. The reaction and purification of the substance is then carried out in the same way as for compound **3**. A dark yellow powder (0.335 g, 47 %) is obtained. MM = 404.49 g/mol, **$C_{25}H_{16}N_4S$**.

MS: m/z: 404 [M^+].

^{1}H NMR (400 MHz, $CDCl_3$) δ: 9.40 (s, **1H**), 9.13 (d, J = 4.7 Hz, **1H**), 8.40 (dd, J = 16.1; 8.3 Hz, **3H**), 7.64 (dd, J = 8.5; 4.2 Hz, **1H**), 7.40 (d, J = 8.2 Hz, **2H**), 7.15 (d, J = 7.6 Hz, **2H**), 7.01 (t, J = 7.7 Hz, **2H**), 6.93 (t, J = 7.5 Hz, **2H**), 6.69 (d, J = 8.0 Hz, **2H**).

^{13}C NMR (101 MHz, $CDCl_3$) δ: 154, 153, 150, 145, 144, 142, 138, 136, 132, 130, 127, 127, 125, 125, 124, 124, 120.

9,9'-(Pyrido[2,3-b]pyrazine-2,3-diylbis(4,1-phenylene))bis(9H-carbazole) (5). 0.375 g (1 equiv.) of **PP-2Br**, 0.284 g (2 equiv.) of carbazole, 0.286 g (3.5 equiv.) of sodium tert-butoxide, 0.039 g (0.05 equiv.) of tris(dibenzylideneacetone)dipalladium(0), 0.020 g (0.05 equiv.) of the ligand XPhos (2-(2-(dicyclohexylphosphine)-2',4',6'-tri-isopropyl-1,1'-biphenyl) and 15 ml of dry degassed toluene was added to a Schlenk flask with a magnetic stirrer. The flask was purged with nitrogen gass and then heated on an electric hotplate. The reaction is then carried out at boiling point for 24 hours. After the reaction, the mixture is cooled and filtered through a glass filter with celite, washed with ethyl acetate and chloroform. The solvents are evaporated and the material obtained is recrystallised from ethyl acetate. Dark brown crystals (0.342 g, 65 %) are obtained. MM = 613.72 g/mol, **$C_{43}H_{27}N_5$**.

MS: m/z: 614 [M+H] $^+$.

^{1}H NMR (400 MHz, $CDCl_3$) δ: 9.27 (d, J = 2.4, Hz, **1H**), 8.62 (d, J = 6.5 Hz, **1H**), 8.16 (d, J = 7.7 Hz, **4H**), 8.01 (d, J = 8.1 Hz, **2H**), 7.94 (d, J = 8.2 Hz, **2H**), 7.81 (dd, J = 8.4; 4.2 Hz, **1H**), 7.70

(dd, J = 11.0; 8.2 Hz, **4H**), 7.50 (d, J = 8.2 Hz, **4H**), 7.43 (t, J = 7.6 Hz, **4H**), 7.32 (t, J = 7.4 Hz, **4H**).

^{13}C NMR (101 MHz, $CDCl_3$) δ: 155, 154, 153, 150, 140, 139, 139, 138, 137, 136, 136, 132, 131, 127, 126, 126, 125, 123, 120, 120, 109, 109.

10,10'-(Pyrido[2,3-*b*]pyrazine-2,3-diylbis(4,1-phenylene))bis(10*H*-phenothiazine) (6). 0.354 g (1 equiv.) of **PP-2Br**, 0.320 g (2 equiv.) of 10*H*-phenothiazine, 0.380 g (5.5 eq.) of sodium tert-butoxide, 0.036 g (0.05 equiv.) of tris(dibenzylideneacetone)dipalladium(0), 0.019 g (0.05 equiv.) of the ligand XPhos (2-(2-(dicyclohexylphosphine)-2',4',6'-tri-isopropyl-1,1'-biphenyl) and 15 ml of dry degassed toluene was added to a Schlenk flask with a magnetic stirrer. The reaction and purification of the substance is then carried out in the same way as for compound **5**. Dark yellowish/orange (0.345 g, 63%) are obtained. MM = 677.84 g/mol, **$C_{43}H_{27}N_5S_2$**.

MS: m/z: 677 [M^+].

^{1}H NMR (400 MHz, $CDCl_3$) δ: 9.22 (d, J = 2.4 Hz, **1H**), 8.56 (d, J = 8.3 Hz, **1H**), 7.80 (d, J = 8.4 Hz, **2H**), 7.75 (d, J = 8.4 Hz, **3H**), 7.34 (dd, J = 16.7; 8.1 Hz, **4H**), 7.13 (t, J = 6.7 Hz, **4H**), 6.95 – 6.82 (m, **8H**), 6.51 (dd, J = 6.0; 3.6 Hz, **2H**), 6.48 (d, J = 7.6 Hz, **2H**).

^{13}C NMR (101 MHz, $CDCl_3$) δ: 155, 154, 154, 150, 143, 143, 143, 143, 138, 136, 136, 136, 132, 132, 127, 127, 127, 127, 127, 126, 125, 124, 123, 123, 118, 118.

Figures

a)

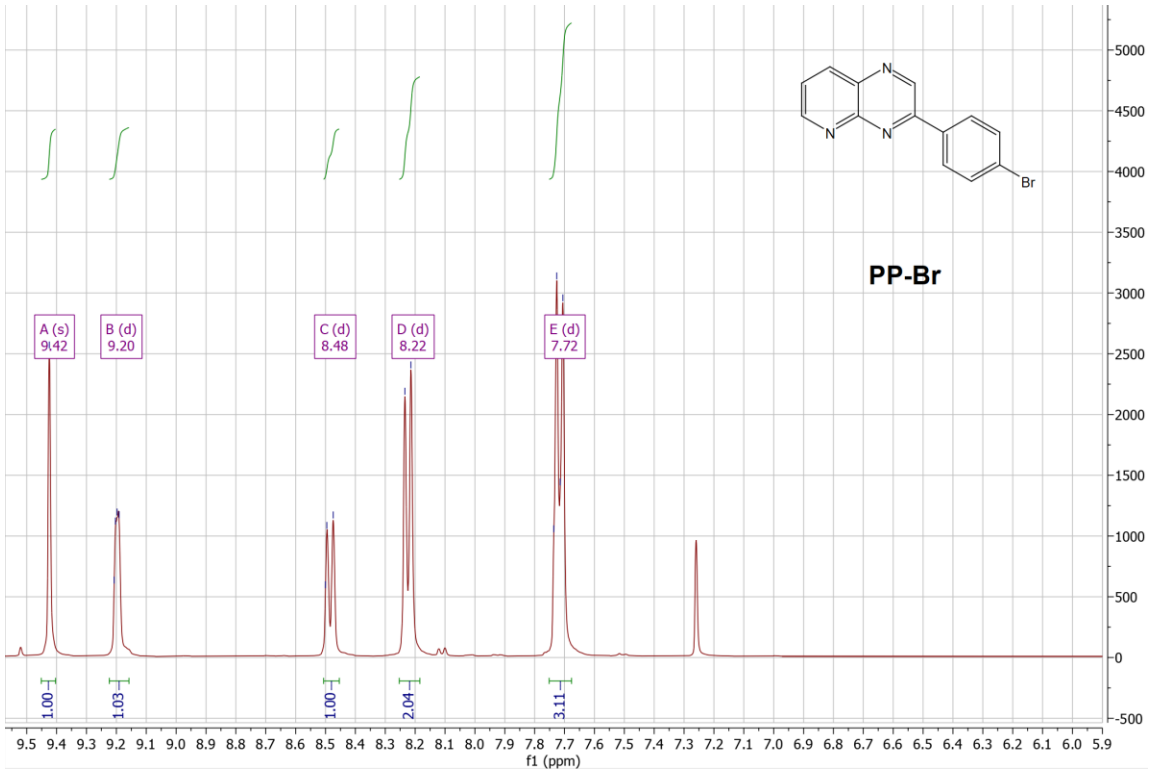

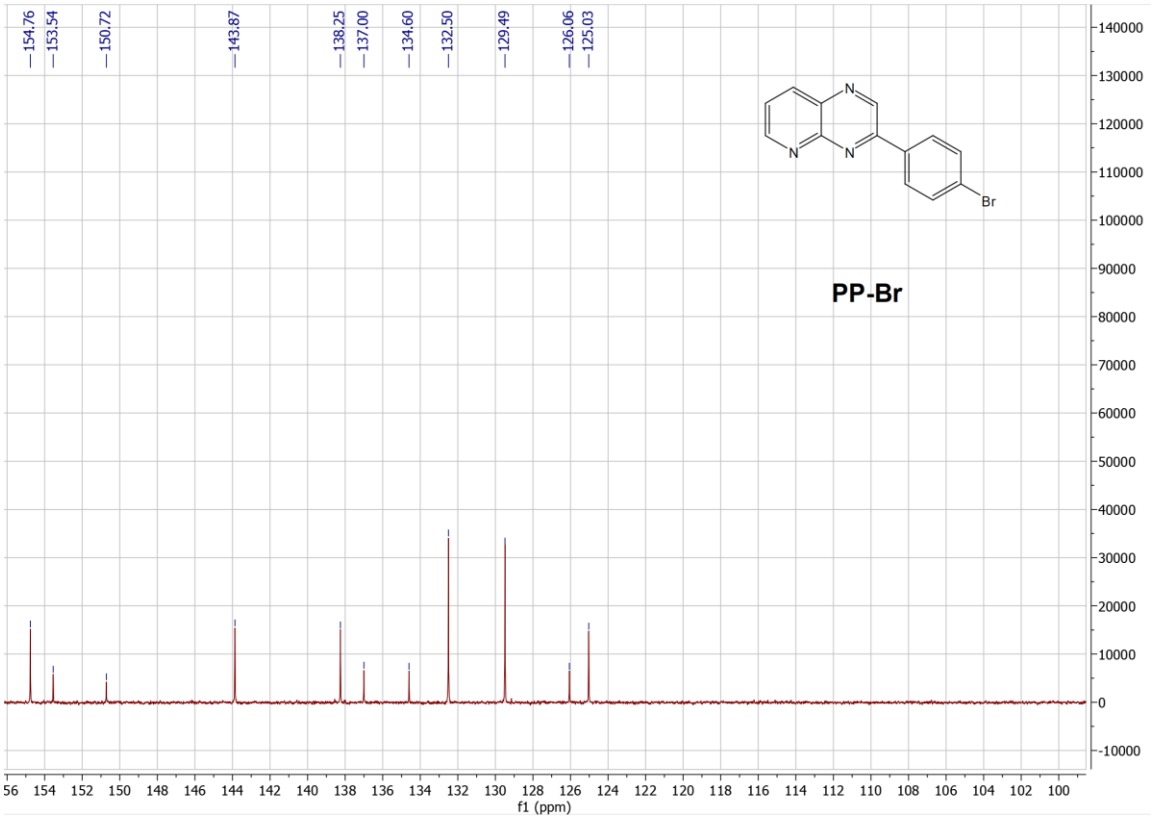
154.76
153.54
150.72
143.87
138.25
137.00
134.60
132.50
129.49
126.06
125.03
N
N
N
Br
PP-Br
f1 (ppm)

b)

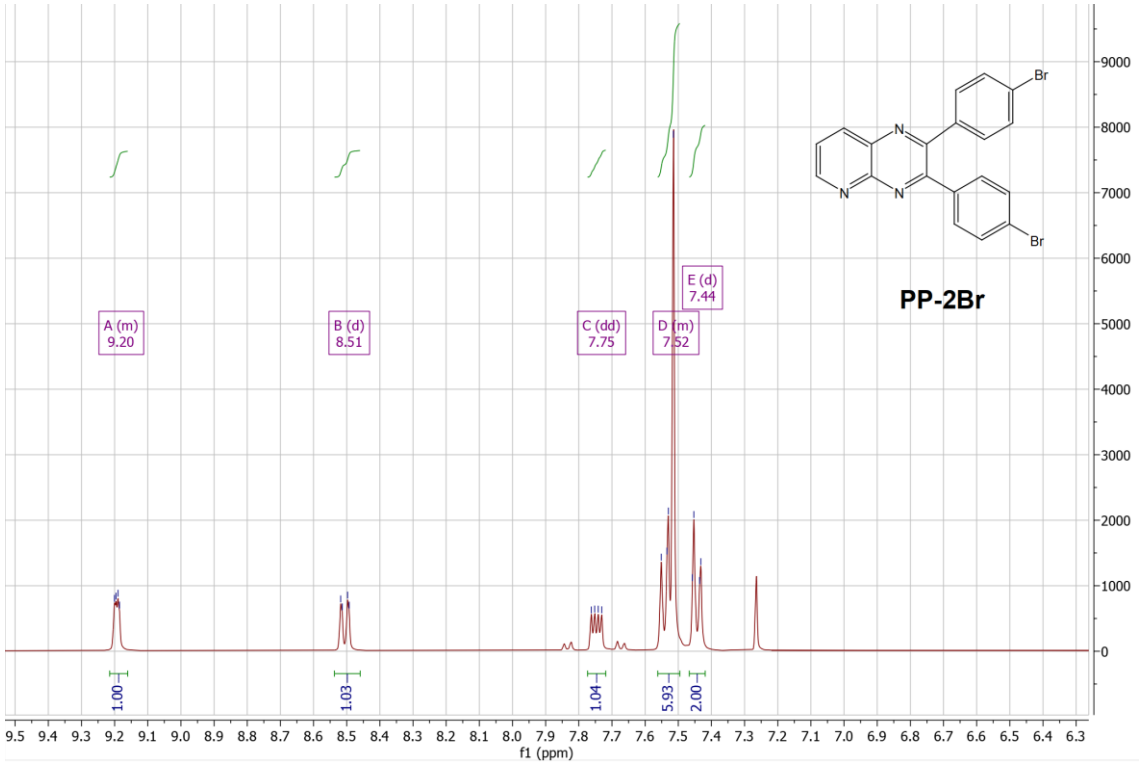
A (m)
9.20
B (d)
8.51
C (dd)
7.75
D (m)
7.52
E (d)
7.44
1.00
1.03
1.04
5.93
2.00
Br
Br
N
N
N
PP-2Br
f1 (ppm)

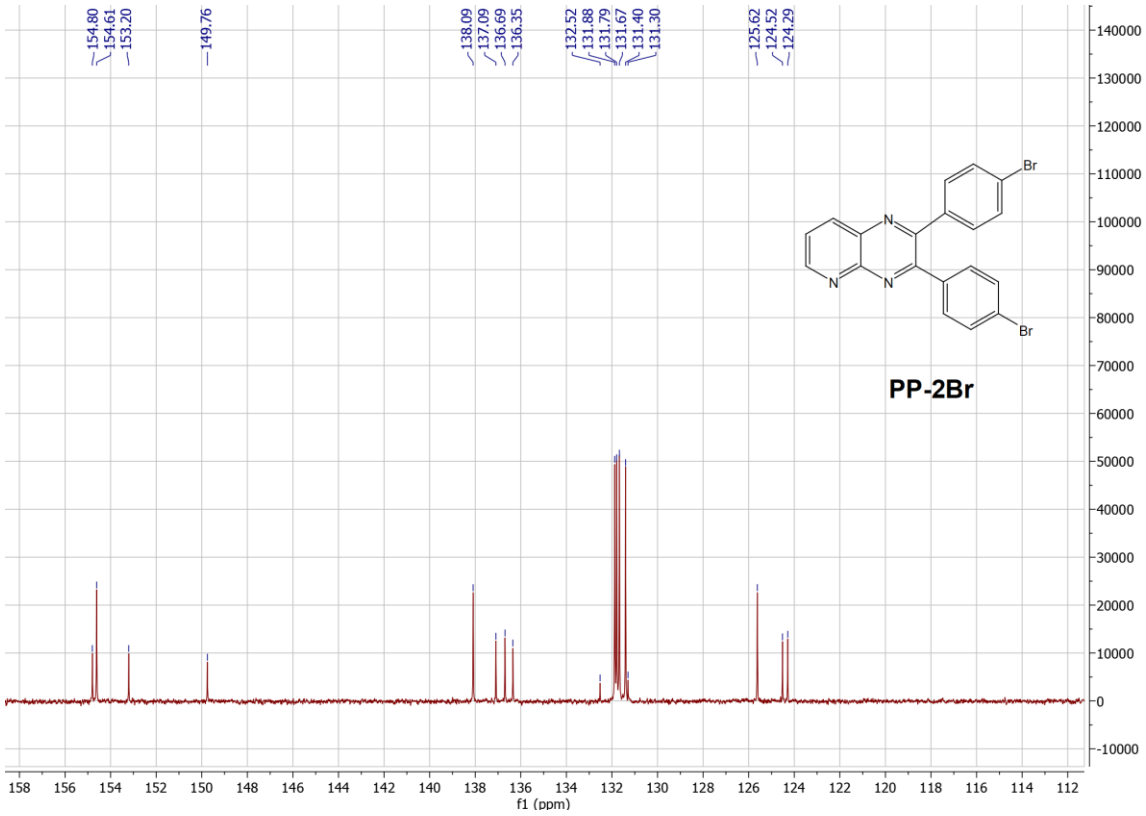
154.80
154.61
153.20
149.76
138.09
137.09
136.69
136.35
132.52
131.88
131.79
131.67
131.40
131.30
125.62
124.52
124.29
Br
Br
PP-2Br
f1 (ppm)

c)

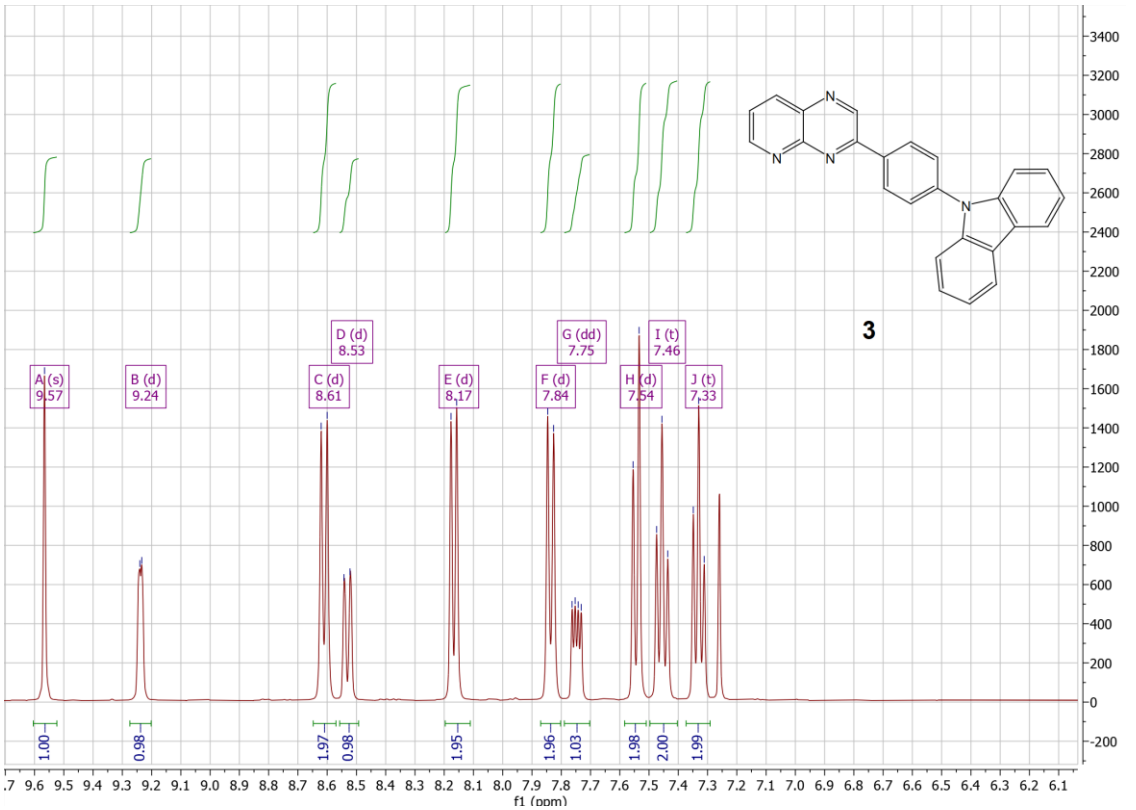
A (s)
9.57
B (d)
9.24
C (d)
8.61
D (d)
8.53
E (d)
8.17
F (d)
7.84
G (dd)
7.75
H (d)
7.54
I (t)
7.46
J (t)
7.33
3
1.00
0.98
1.97
0.98
1.95
1.96
1.03
1.98
2.00
1.99
f1 (ppm)

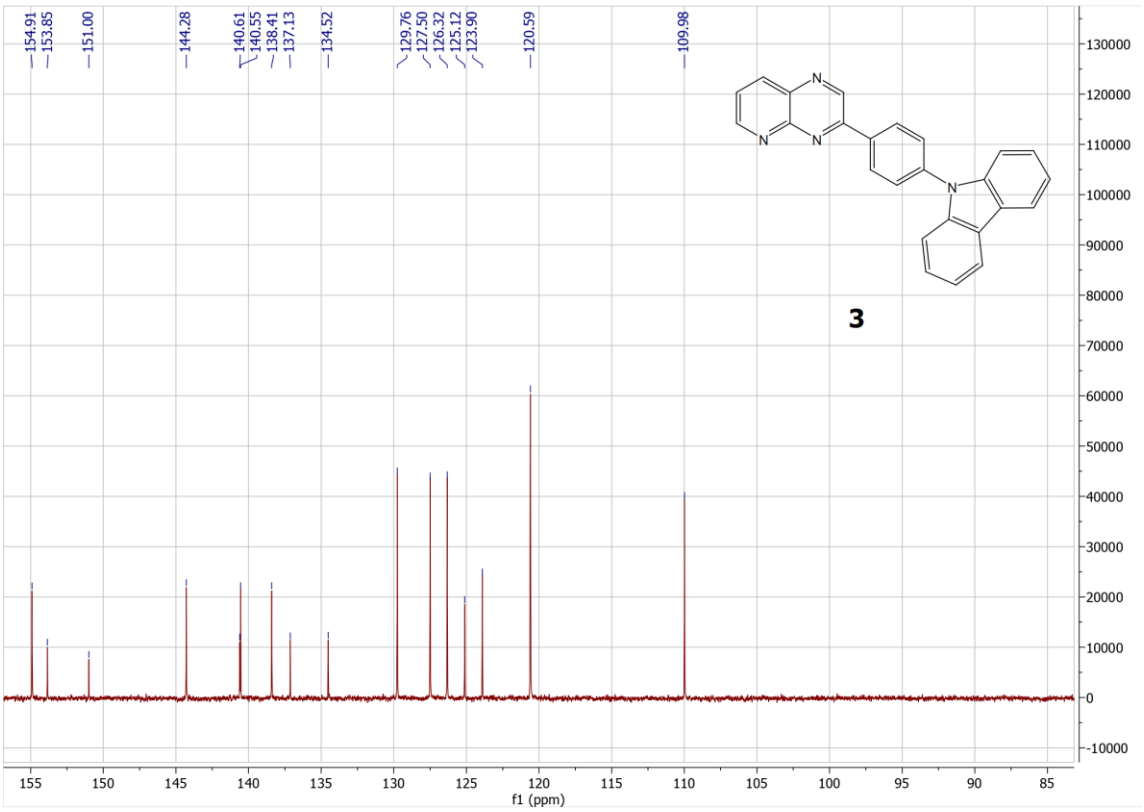
154.91
153.85
151.00
144.28
140.61
140.55
138.41
137.13
134.52
129.76
127.50
126.32
125.12
123.90
120.59
109.98
3
f1 (ppm)

d)

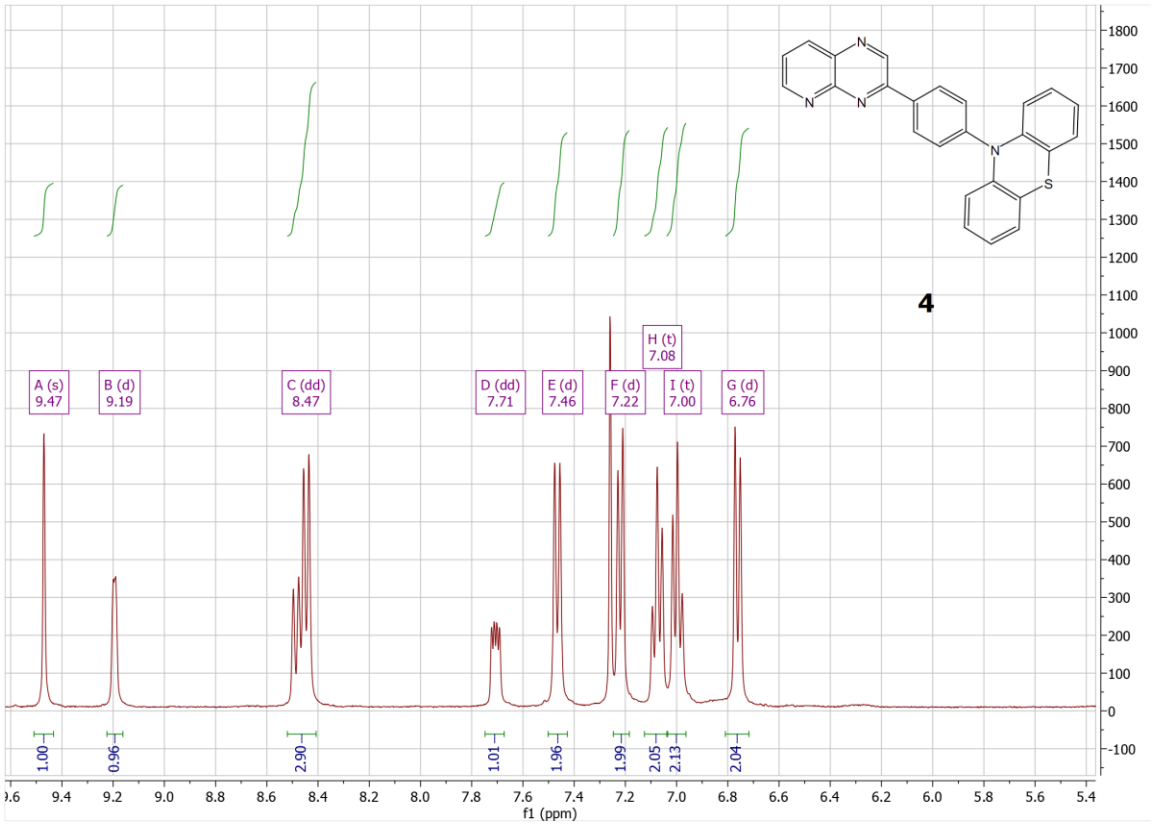
A (s) 9.47
B (d) 9.19
C (dd) 8.47
D (dd) 7.71
E (d) 7.46
F (d) 7.22
H (t) 7.08
I (t) 7.00
G (d) 6.76
1.00
0.96
2.90
1.01
1.96
1.99
2.05
2.13
2.04
4
f1 (ppm)

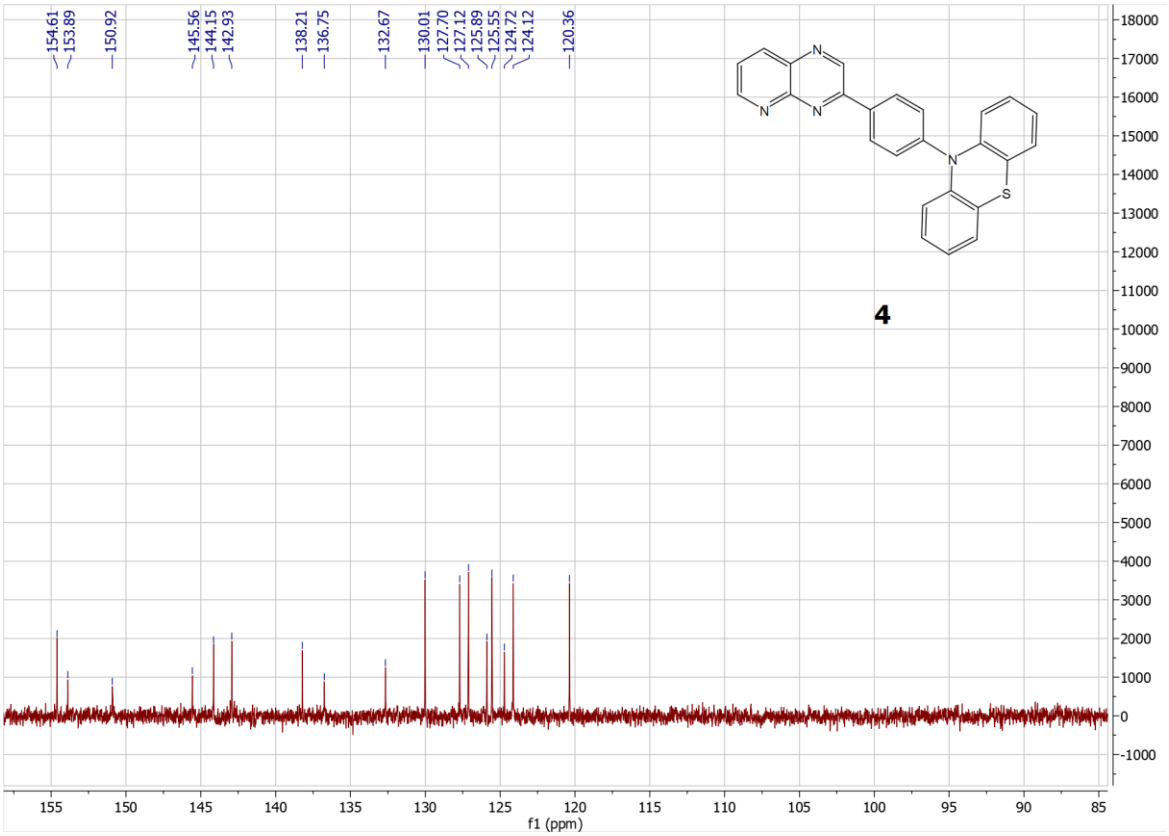
154.61
153.89
150.92
145.56
144.15
142.93
138.21
136.75
132.67
130.01
127.70
127.12
125.89
125.55
124.72
124.12
120.36
4
f1 (ppm)

e)

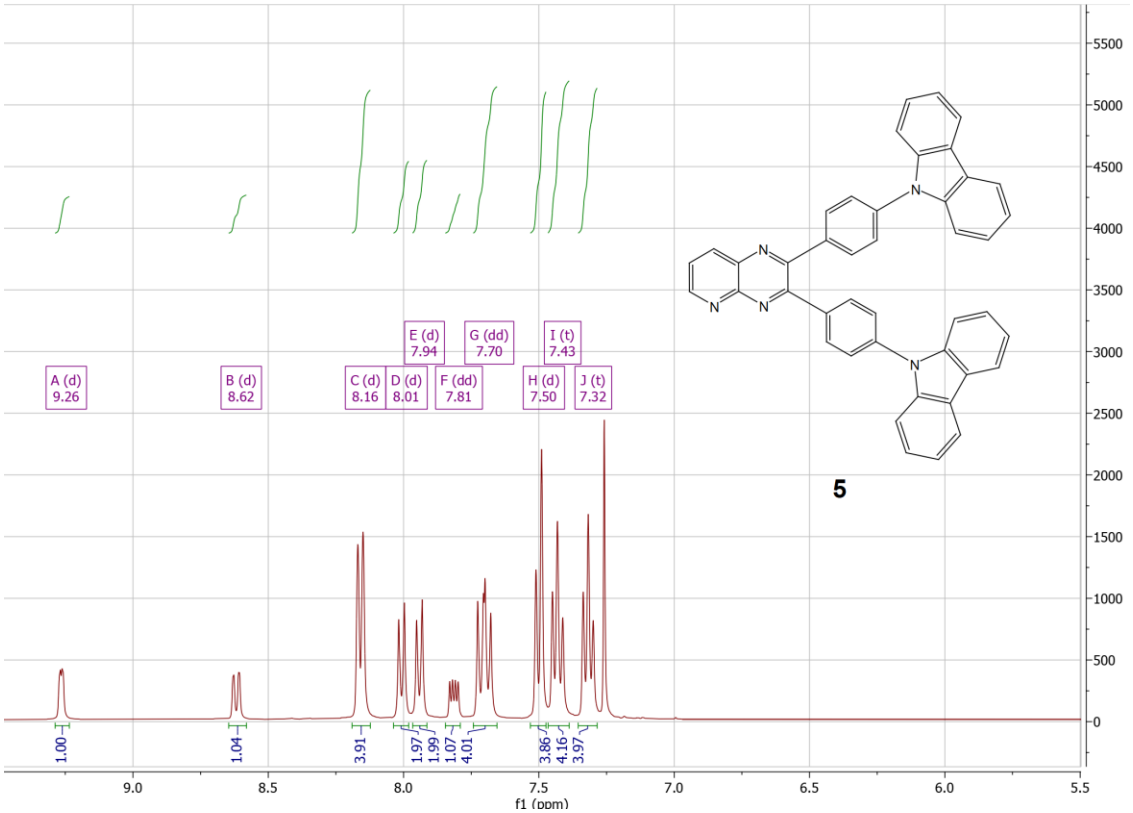
A (d) 9.26
B (d) 8.62
C (d) 8.16
D (d) 8.01
E (d) 7.94
F (dd) 7.81
G (dd) 7.70
H (d) 7.50
I (t) 7.43
J (t) 7.32
1.00
1.04
3.91
1.97
1.99
1.07
4.01
3.86
4.16
3.97
5
f1 (ppm)

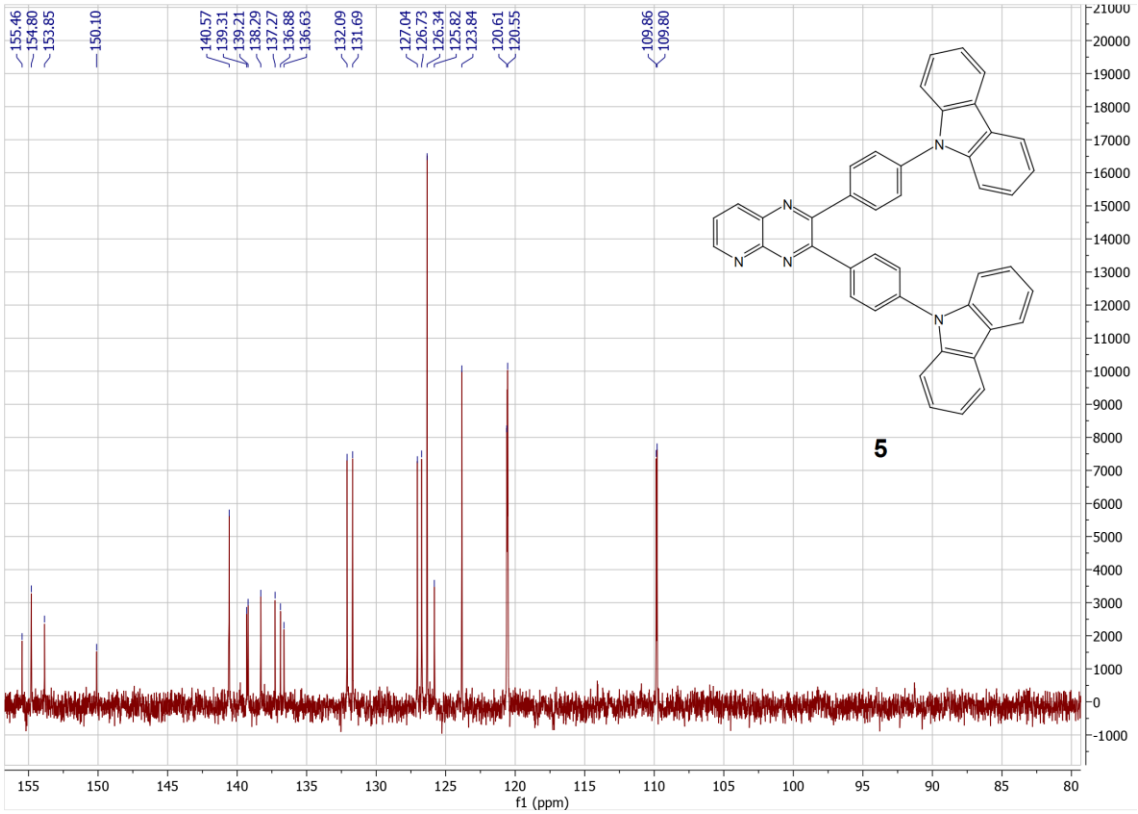
155.46
154.80
153.85
150.10
140.57
139.31
139.21
138.29
137.27
136.88
136.63
132.09
131.69
127.04
126.73
126.34
125.82
123.84
120.61
120.55
109.86
109.80
5
f1 (ppm)

f)

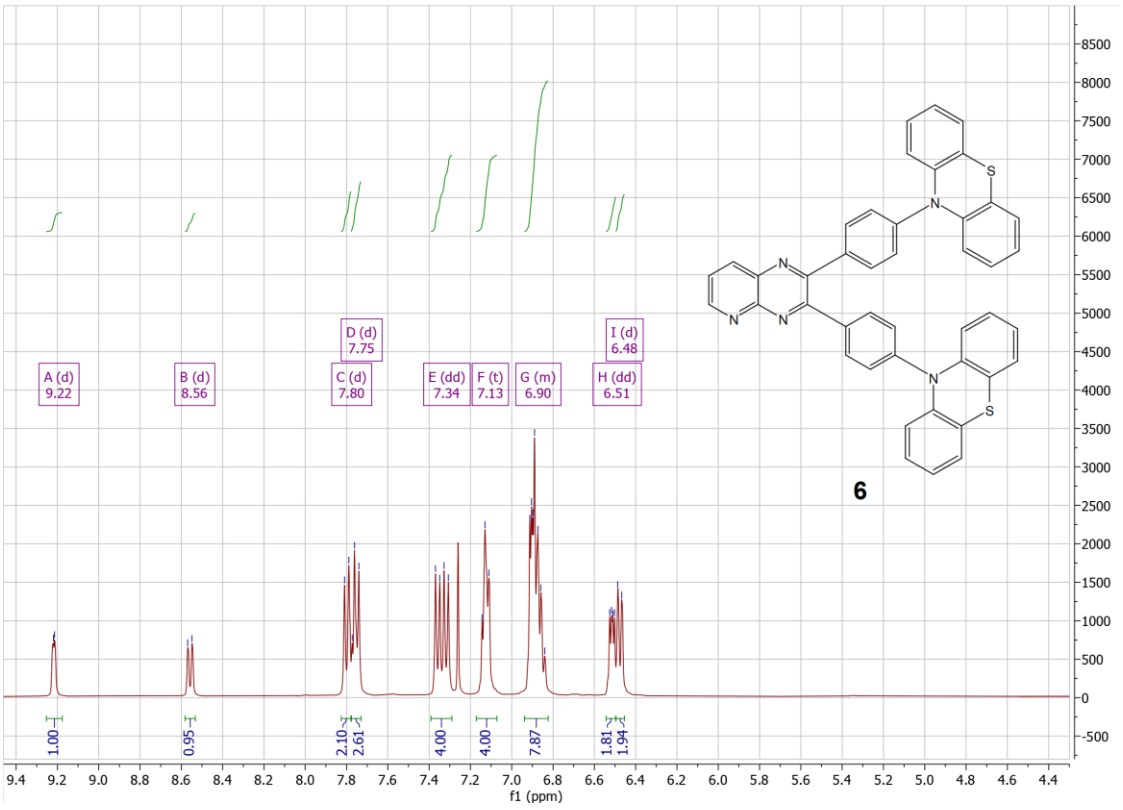
A (d) 9.22
B (d) 8.56
C (d) 7.80
D (d) 7.75
E (dd) 7.34
F (t) 7.13
G (m) 6.90
H (dd) 6.51
I (d) 6.48
1.00
0.95
2.10
2.61
4.00
4.00
7.87
1.81
1.94
6
f1 (ppm)

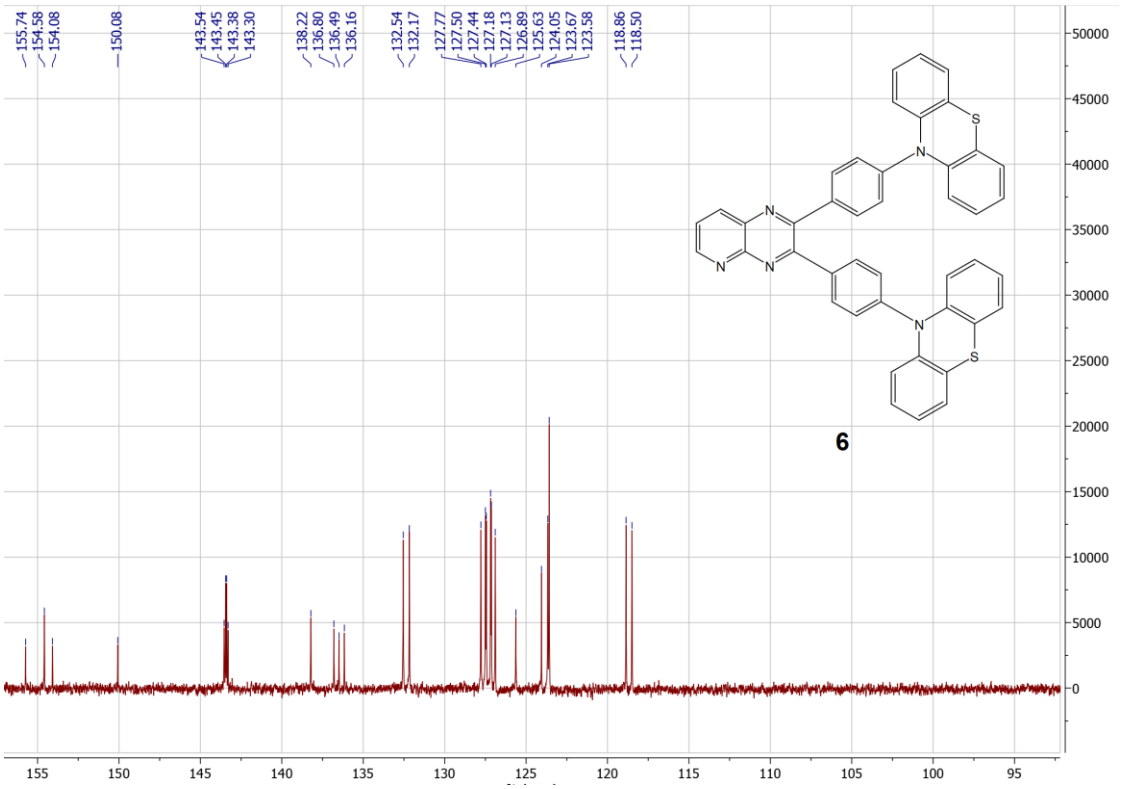

Figure S1. ^{1}H and ^{13}C NMR spectra of: a) **PP-Br**; b) **PP-2Br**; c) **3**; d) **4;** e) **5**; f) **6**.

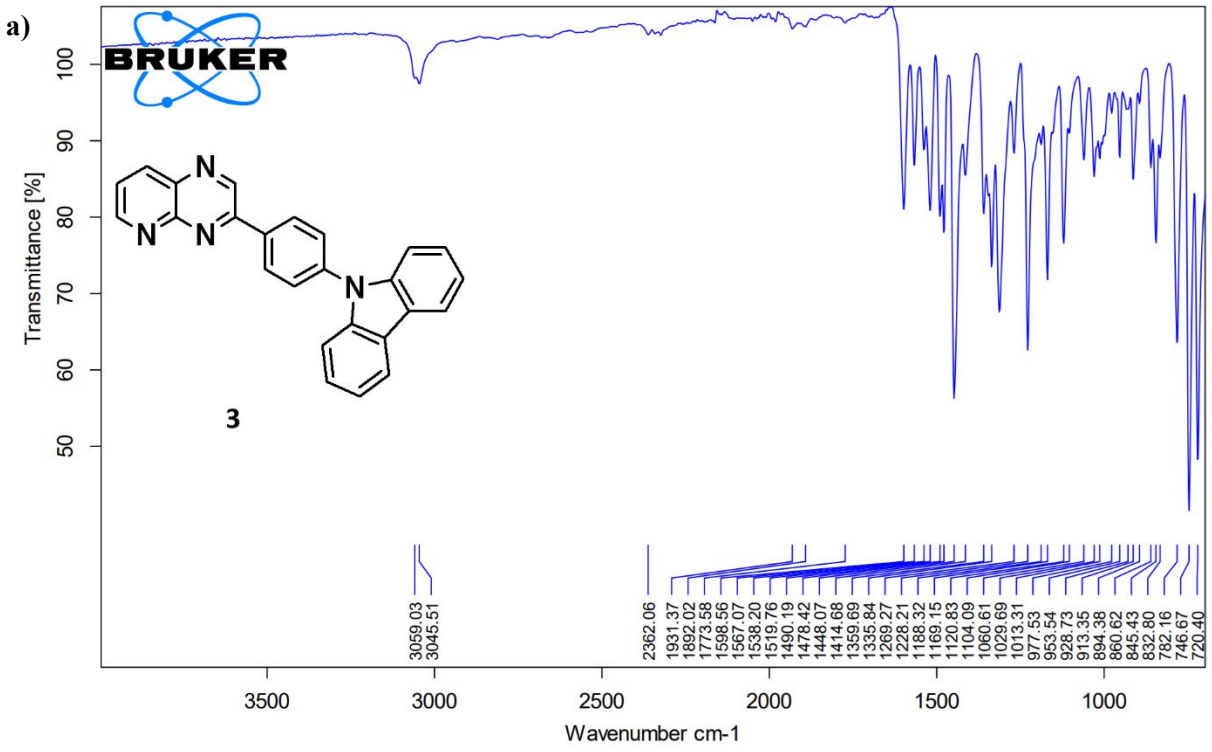

b)

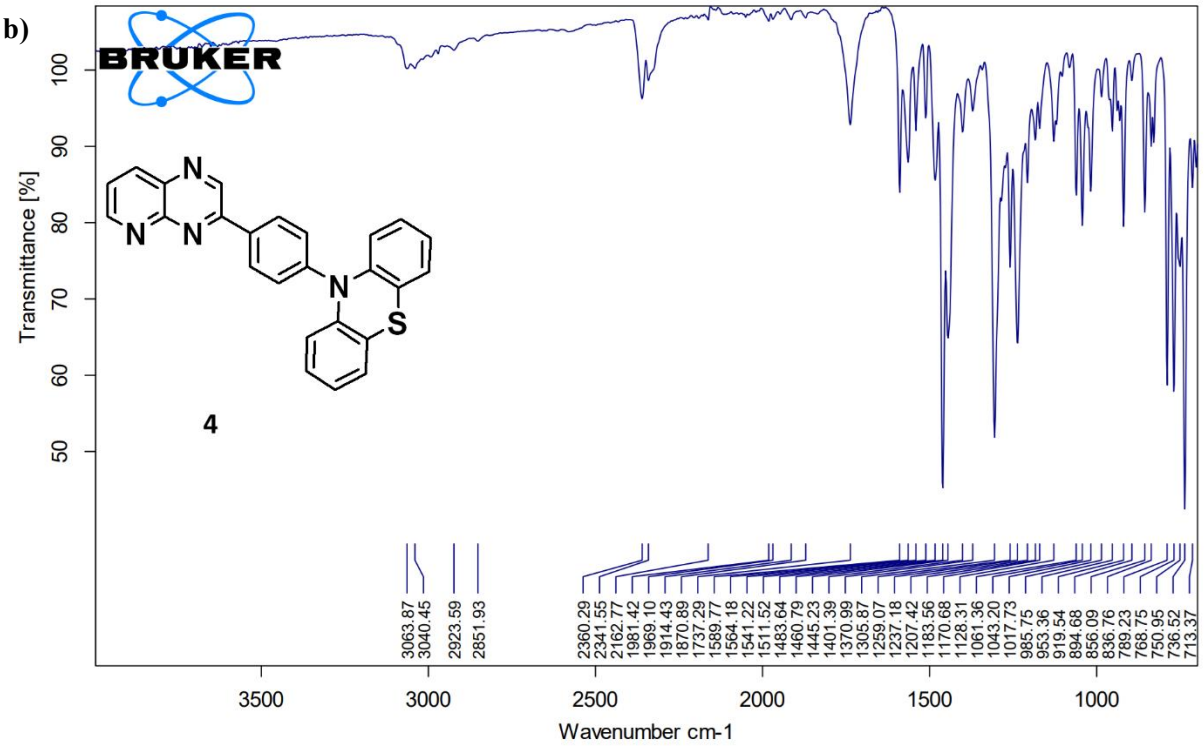
BRUKER
Transmittance [%]
100
90
80
70
60
50
4
3063.87
3040.45
2923.59
2851.93
2360.29
2341.55
2162.77
1981.42
1969.10
1914.43
1870.89
1737.29
1589.77
1564.18
1541.22
1511.52
1483.64
1460.79
1445.23
1401.39
1370.99
1305.87
1259.07
1237.18
1207.42
1183.56
1170.68
1128.31
1061.36
1043.20
1017.73
985.75
953.36
919.54
894.68
856.09
836.76
789.23
768.75
750.95
736.52
713.37
3500
3000
2500
2000
1500
1000
Wavenumber cm-1

c)

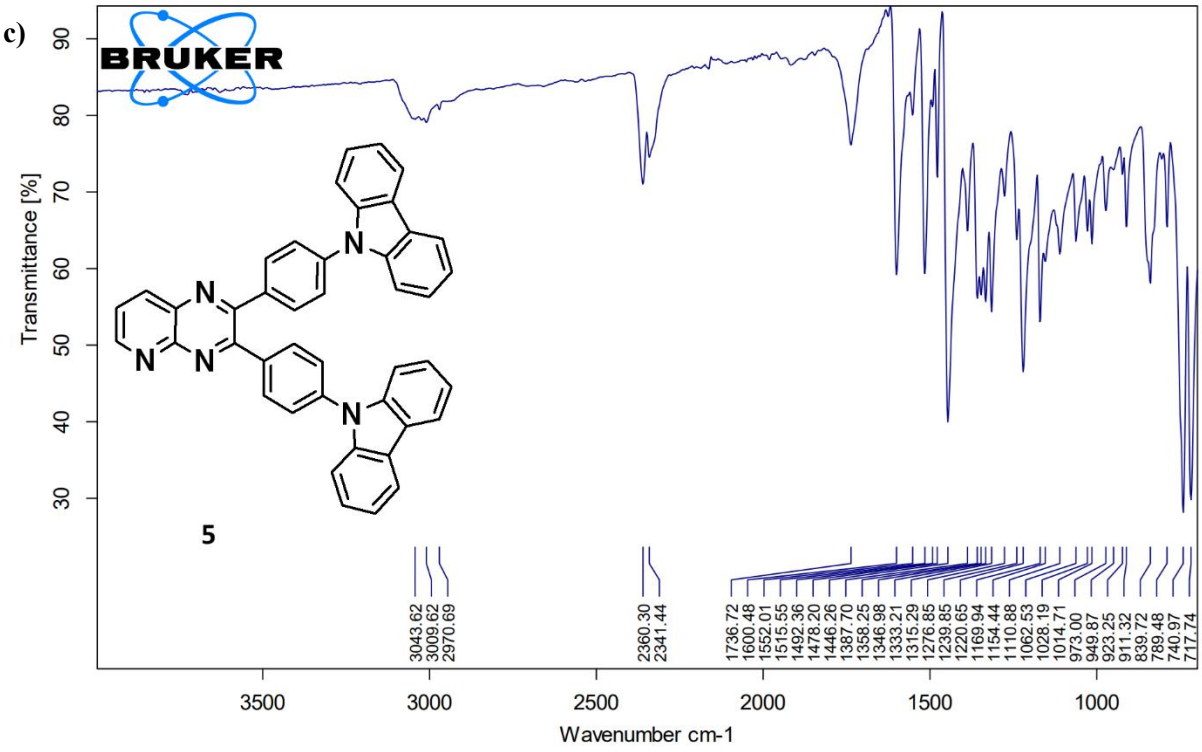
BRUKER
Transmittance [%]
90
80
70
60
50
40
30
5
3043.62
3009.62
2970.69
2360.30
2341.44
1736.72
1600.48
1552.01
1515.55
1492.36
1478.20
1446.26
1387.70
1358.25
1346.98
1333.21
1315.29
1276.85
1239.85
1220.65
1169.94
1154.44
1110.88
1062.53
1028.19
1014.71
973.00
949.87
923.25
911.32
839.72
789.48
740.97
717.74
3500
3000
2500
2000
1500
1000
Wavenumber cm-1

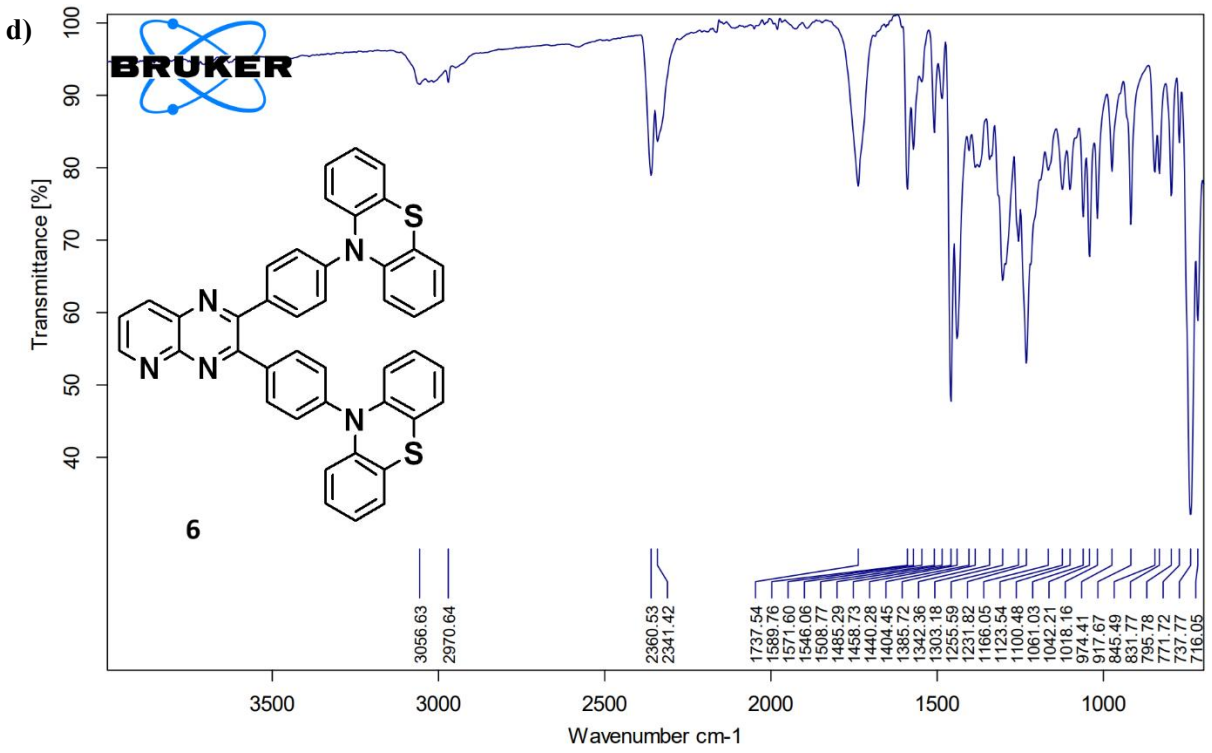

Figure S2. IR spectra of: a) **3**; b) **4**; c) **5**; d) **6**.

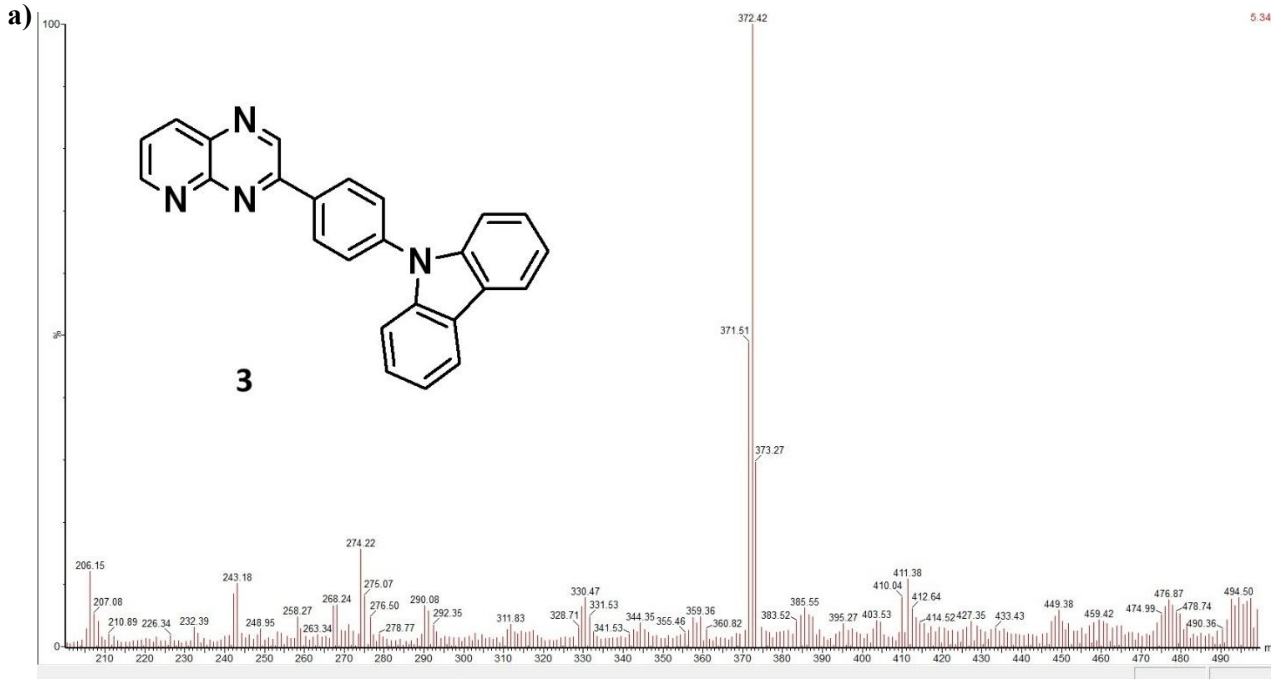

b)

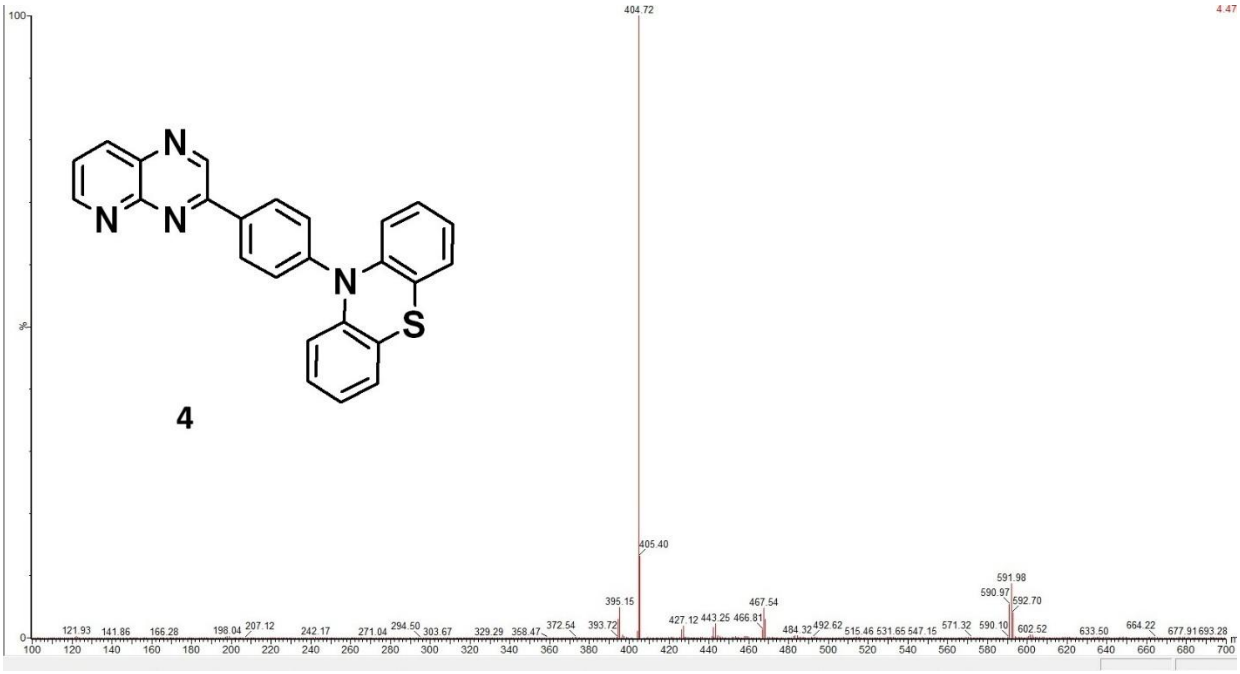
404.72
4.47
405.40
591.98
590.97
592.70
395.15
467.54
427.12
443.25
466.81
4

c)

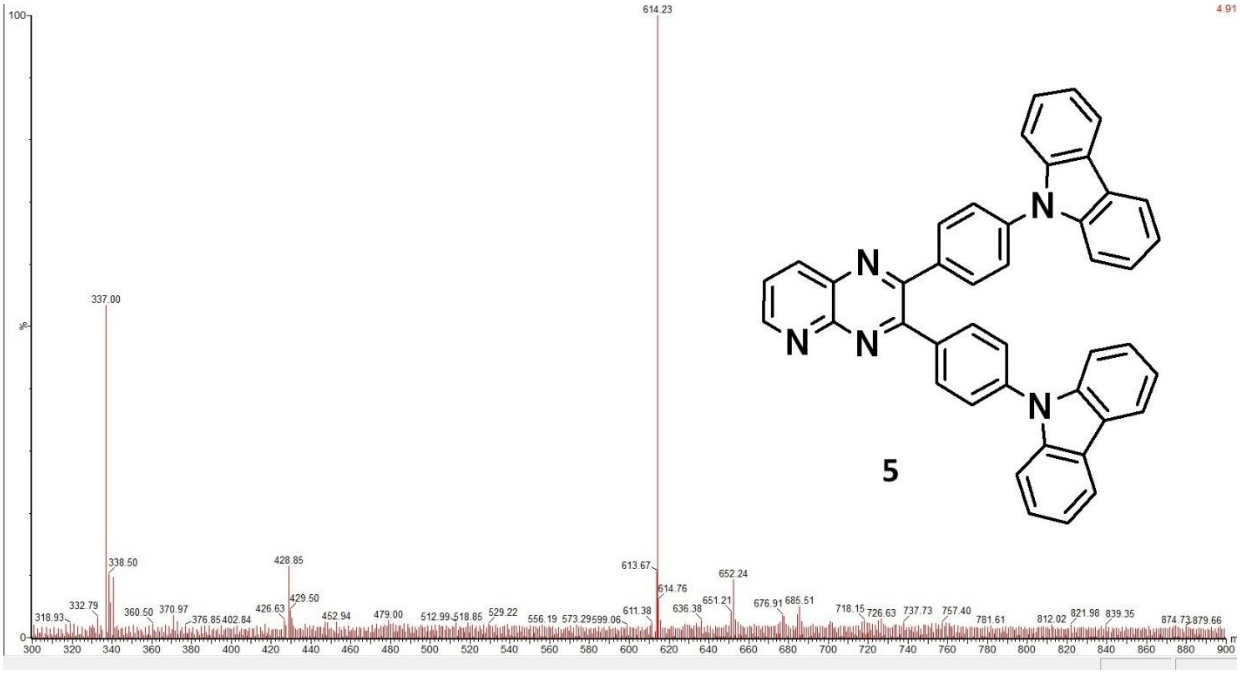
614.23
4.91
337.00
338.50
428.85
613.67
652.24
614.76
429.50
5

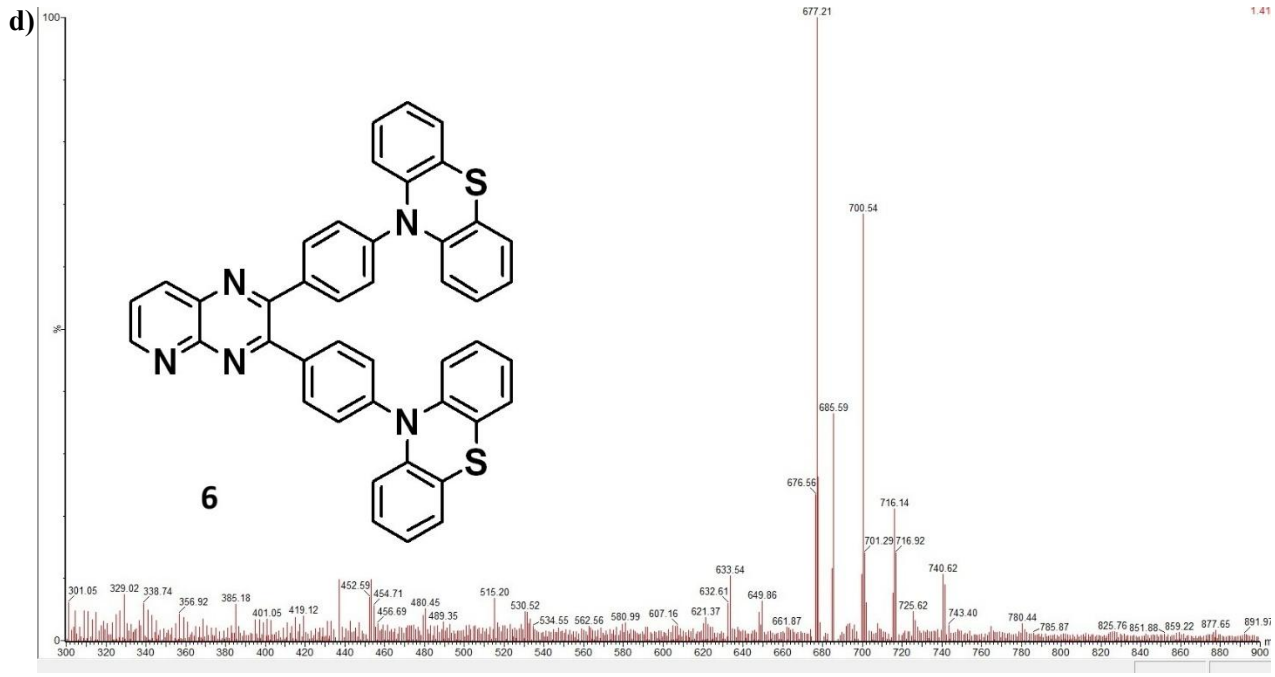

Figure S3. Mass spectra of: a) **3**; b) **4**; c) **5**; d) **6**.

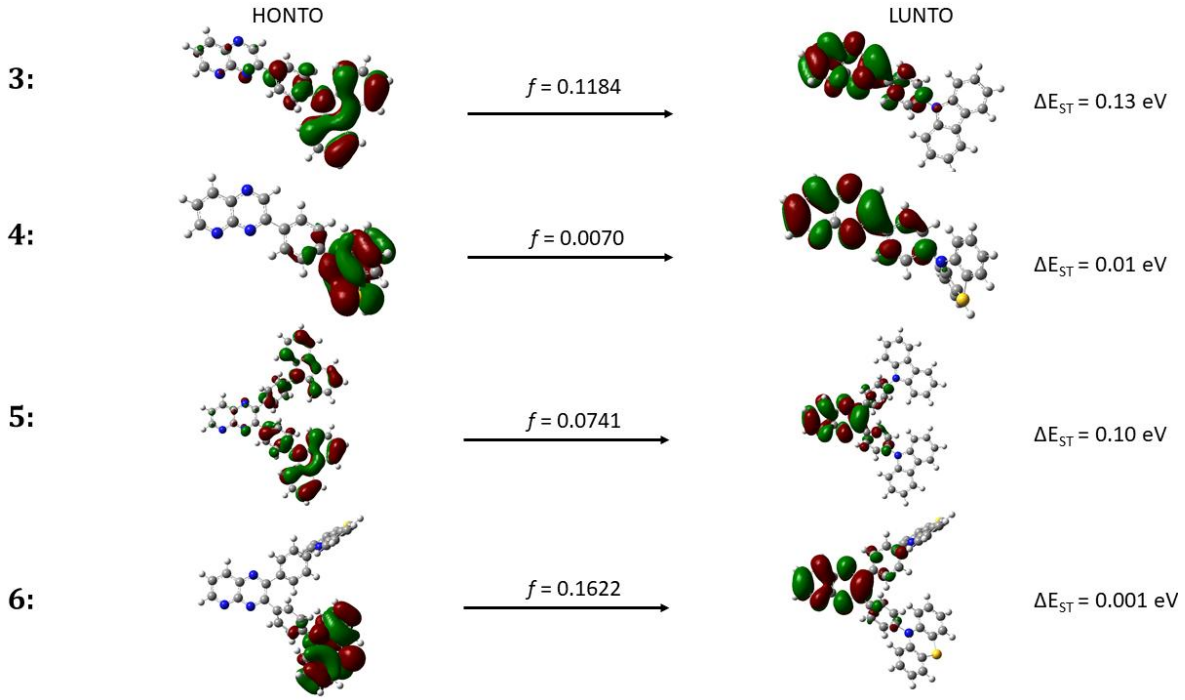

Figure S4. Natural transition orbitals of the 1st excited singlet state of compounds **3–6.**

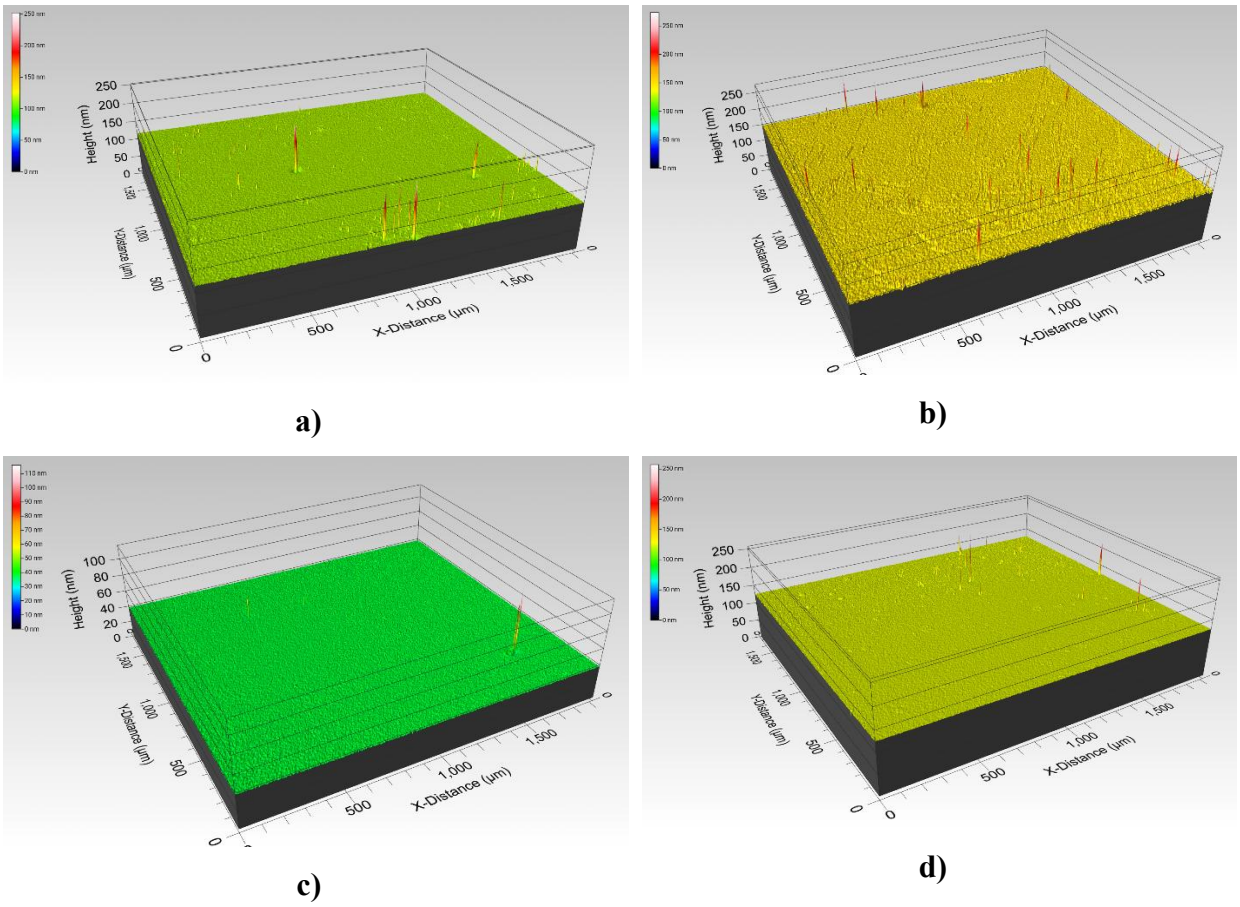

Figure S5. Surface morphology of compound samples (a – **3**; b – **4**; c – **5**; d – **6**).

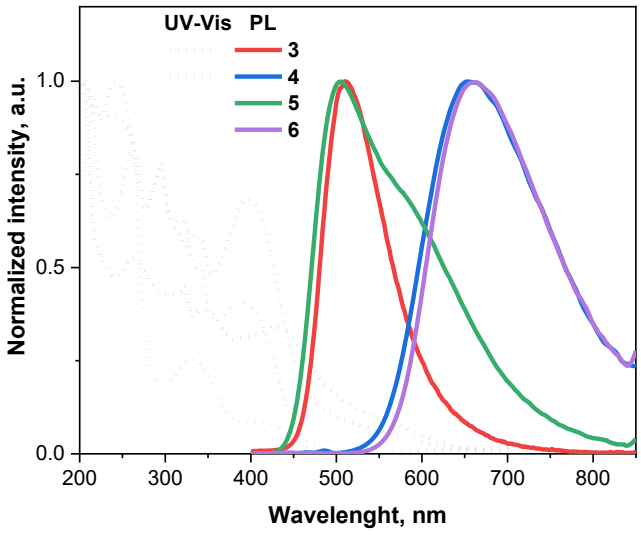

Figure S6. PL spectra of thin films of compounds **3–6**

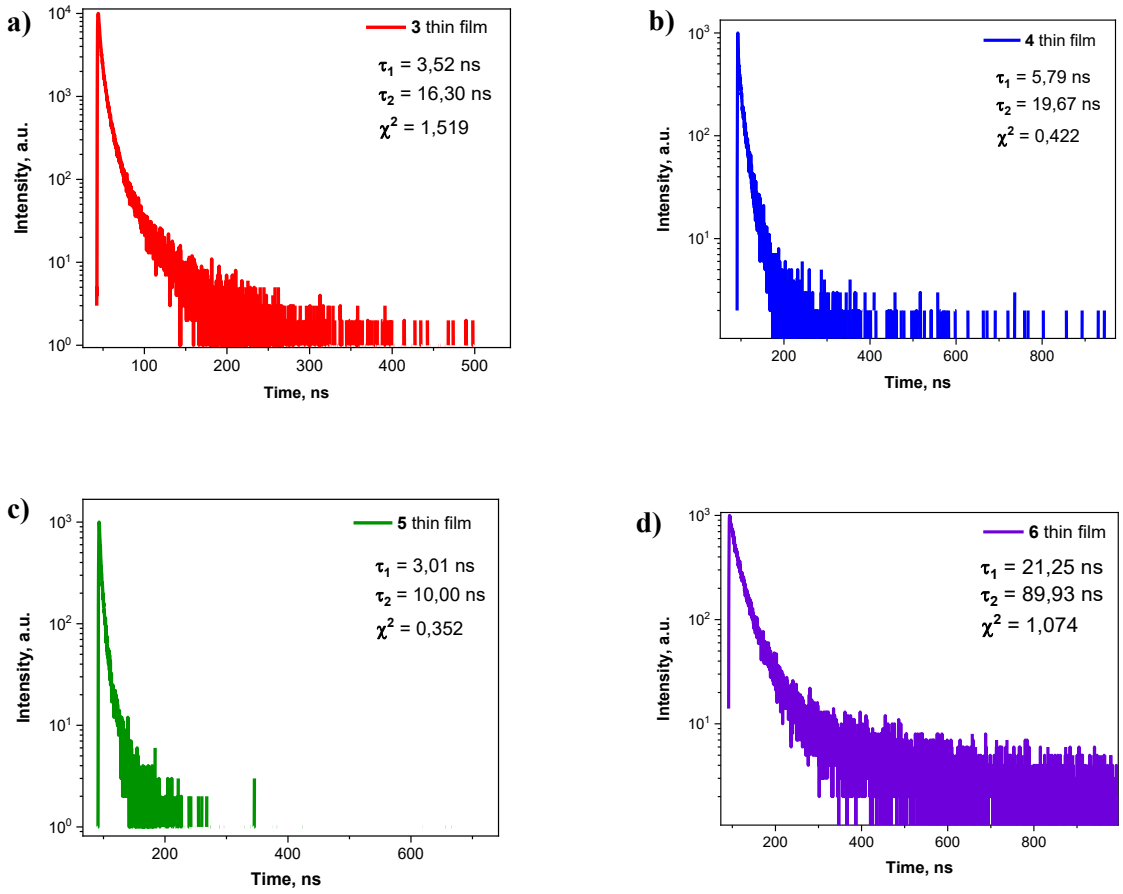

Figure S7. Emission lifetime curves of solid samples of compounds (a – **3**; b – **4**; c – **5**; d – **6**)

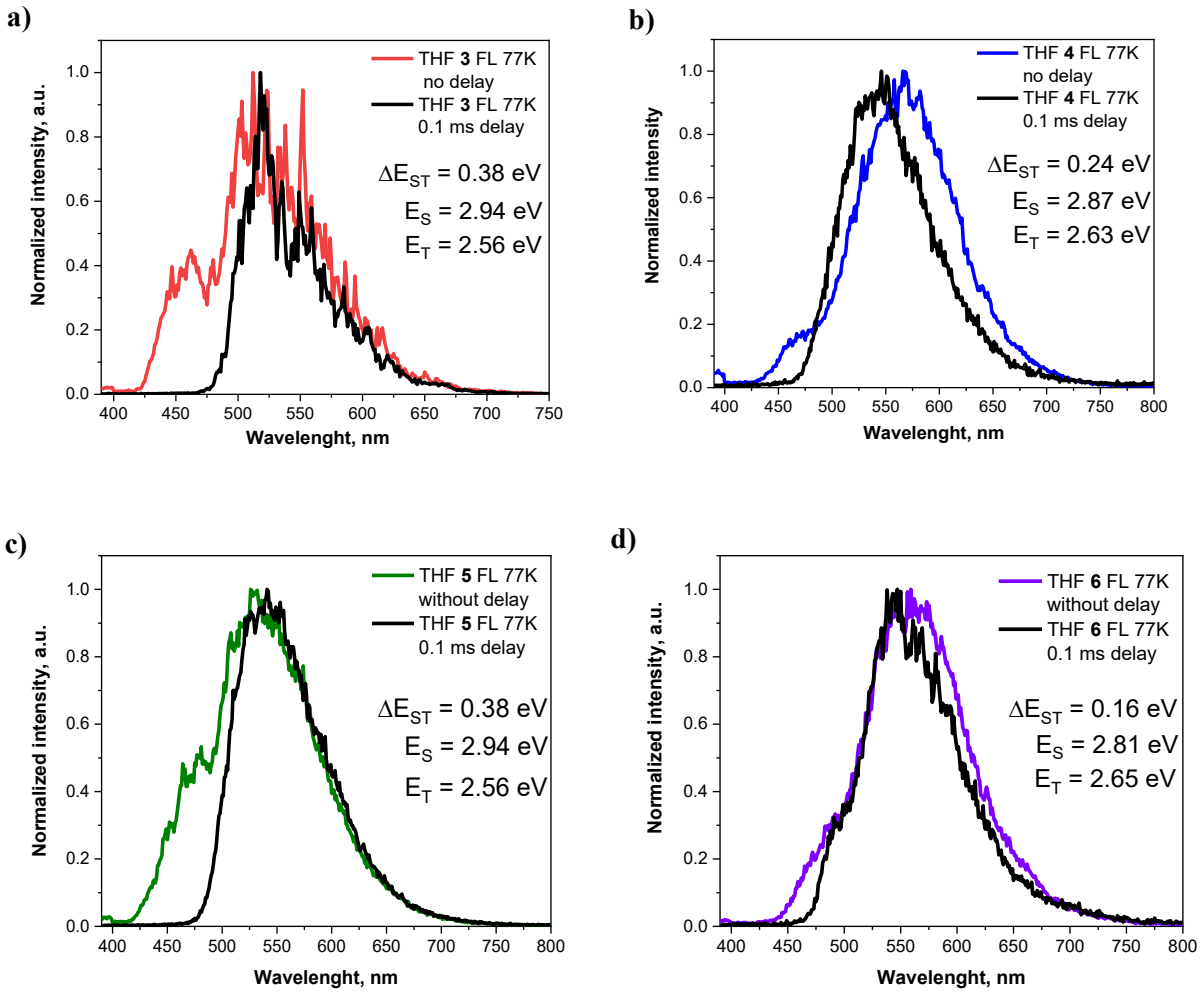

Figure S8. Photoluminescence and phosphorescence spectra of compounds (a – **3**; b – **4**; c – **5**; d – **6**) at 77K

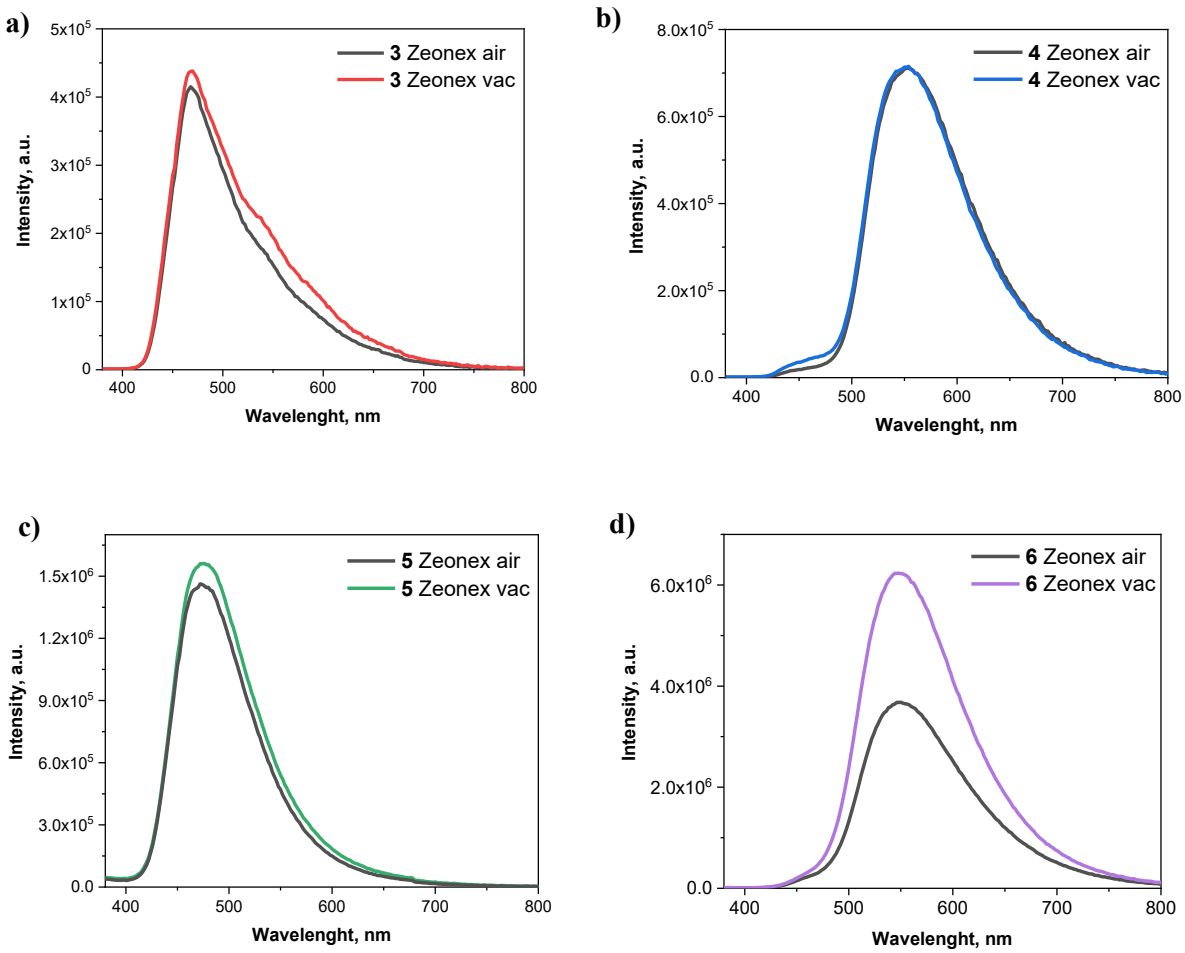

Figure S9. PL spectra of compound (a – **3**; b – **4**; c – **5**; d – **6**) Zeonex thin films in air and in vacuum

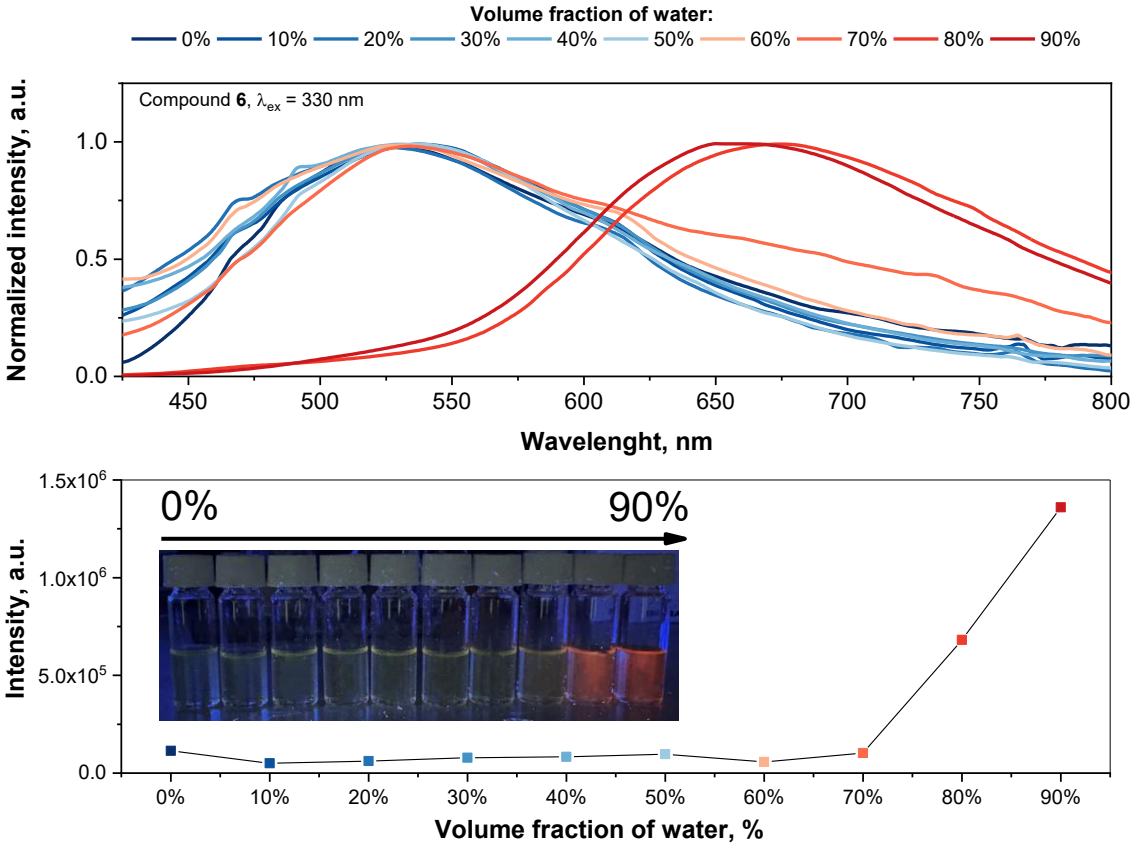

Figure S10. Solvent polarity and aggregation-dependent photoluminescence spectra and emission intensity of compound 6 (H_2O in THF mixtures)

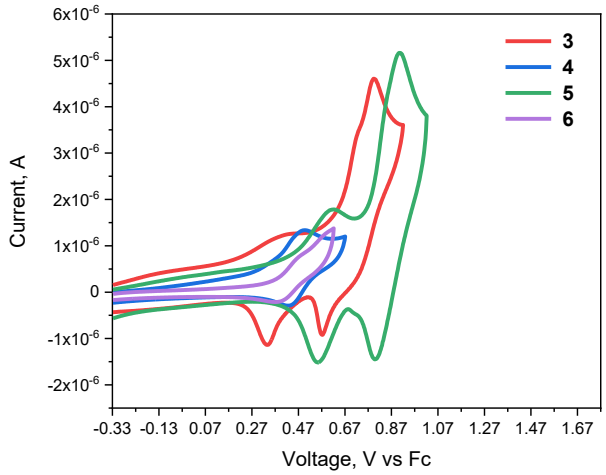

Figure S11. Cyclic voltammograms of compounds (3-6) in 0.1 M NBu_4PF_6/DCM

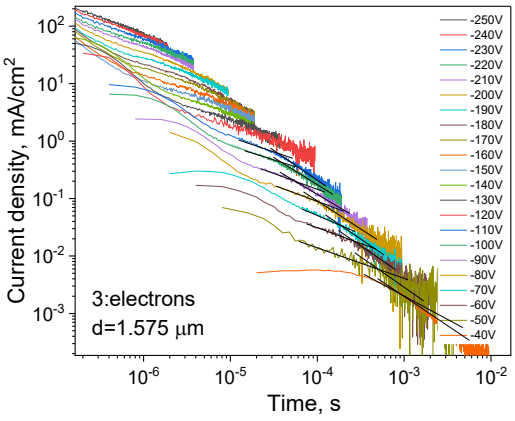
Current density, mA/cm2
Time, s
3:electrons
d=1.575 μm
-250V
-240V
-230V
-220V
-210V
-200V
-190V
-180V
-170V
-160V
-150V
-140V
-130V
-120V
-110V
-100V
-90V
-80V
-70V
-60V
-50V
-40V

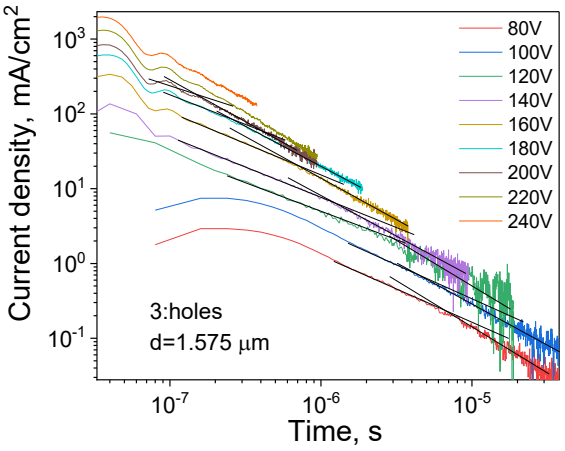
Current density, mA/cm2
Time, s
3:holes
d=1.575 μm
80V
100V
120V
140V
160V
180V
200V
220V
240V

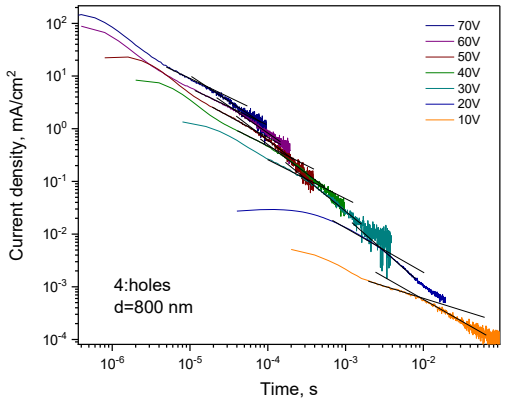
Current density, mA/cm2
Time, s
4:holes
d=800 nm
70V
60V
50V
40V
30V
20V
10V

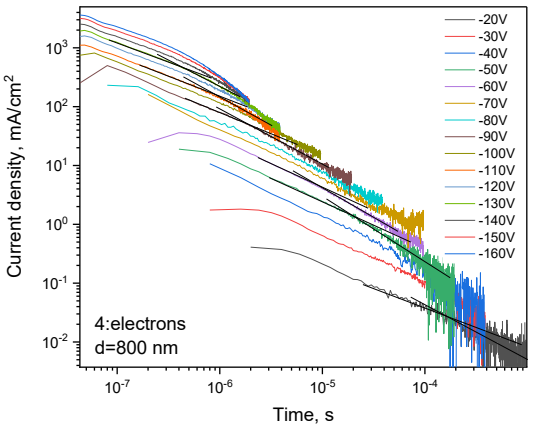
Current density, mA/cm2
Time, s
4:electrons
d=800 nm
-20V
-30V
-40V
-50V
-60V
-70V
-80V
-90V
-100V
-110V
-120V
-130V
-140V
-150V
-160V

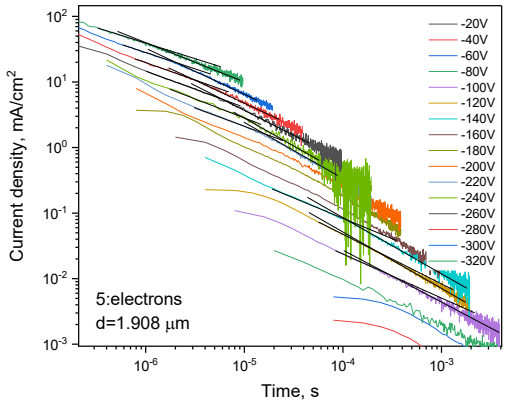
Current density, mA/cm2
Time, s
5:electrons
d=1.908 μm
-20V
-40V
-60V
-80V
-100V
-120V
-140V
-160V
-180V
-200V
-220V
-240V
-260V
-280V
-300V
-320V

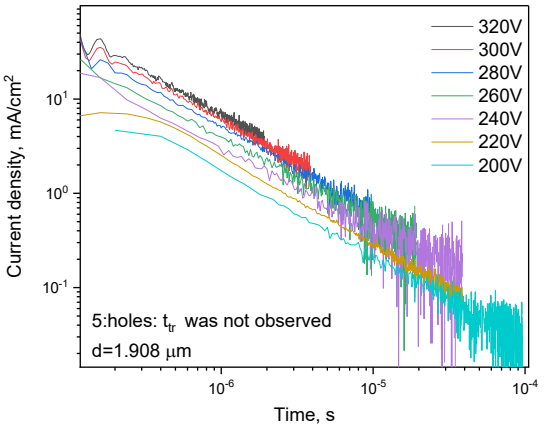
Current density, mA/cm2
Time, s
5:holes: t_tr was not observed
d=1.908 μm
320V
300V
280V
260V
240V
220V
200V

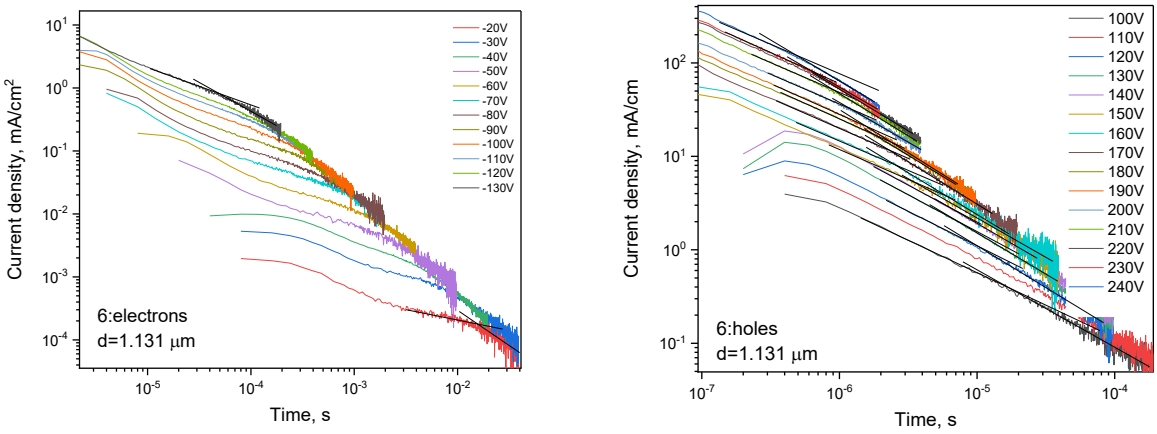

Figure S12. TOF signals for holes or electrons in the vacuum-deposited films.

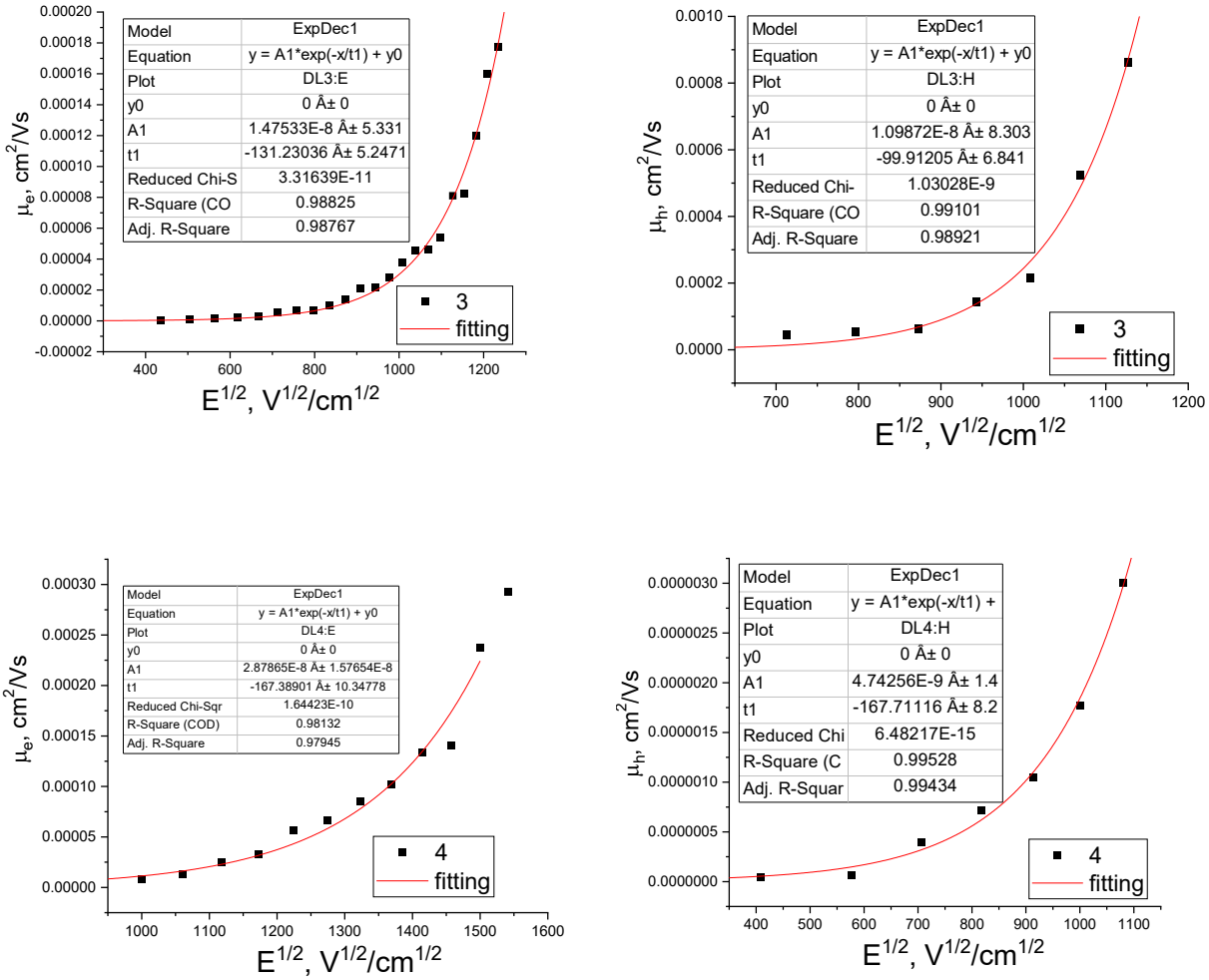

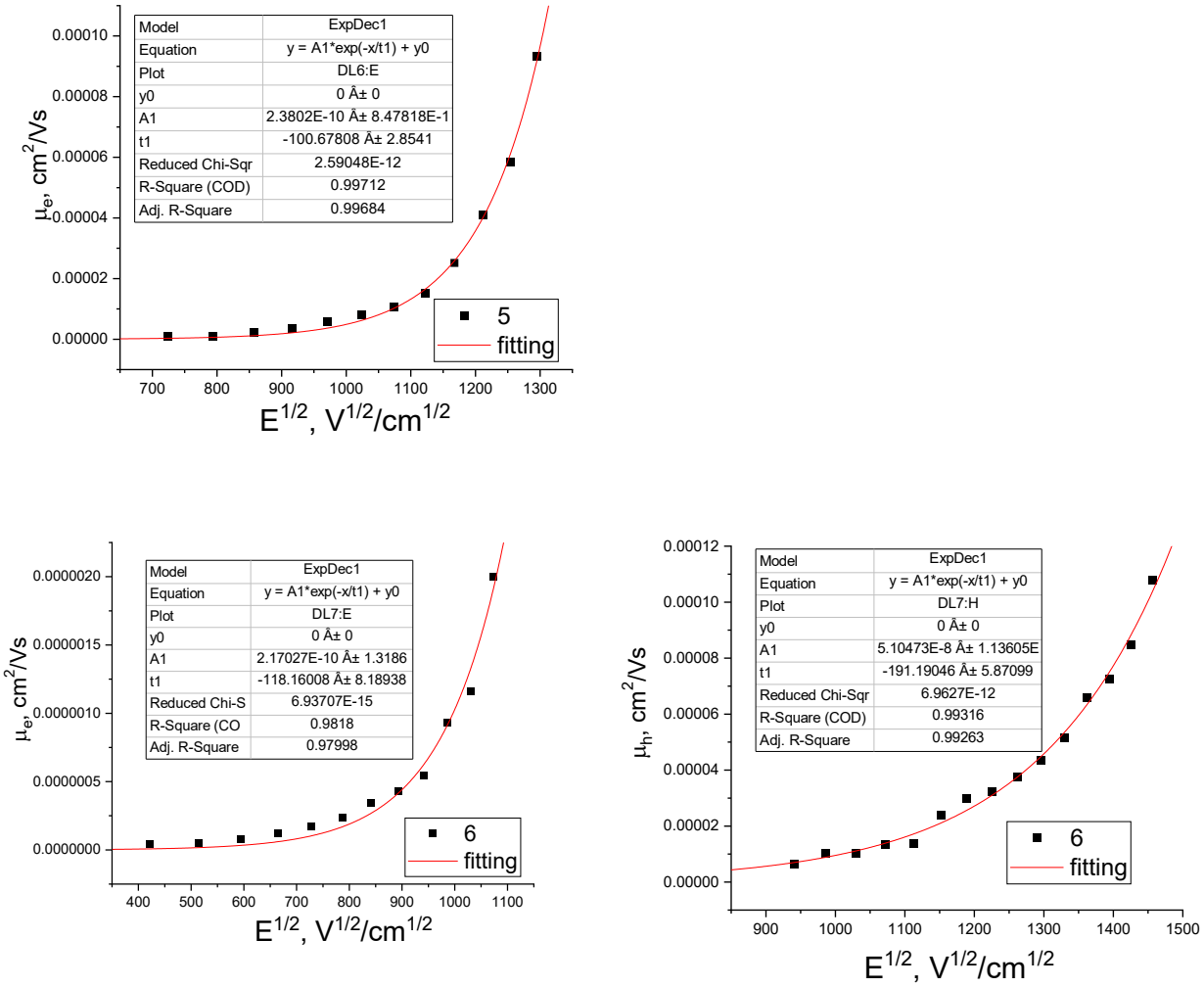

Figure S13. The fitting data for μ_h and μ_e dependents (Figure 6) according to formula (3).

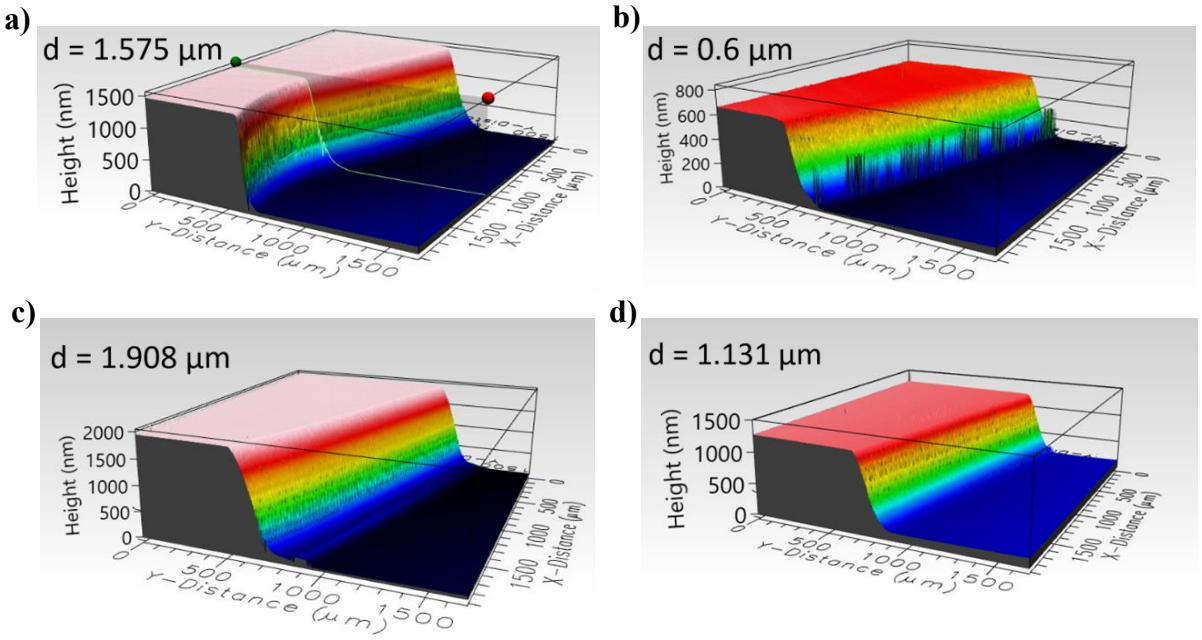

Figure S14. Thickness measurements for TOF samples of **3** (a), **4** (b), **5** (c), **6** (d).

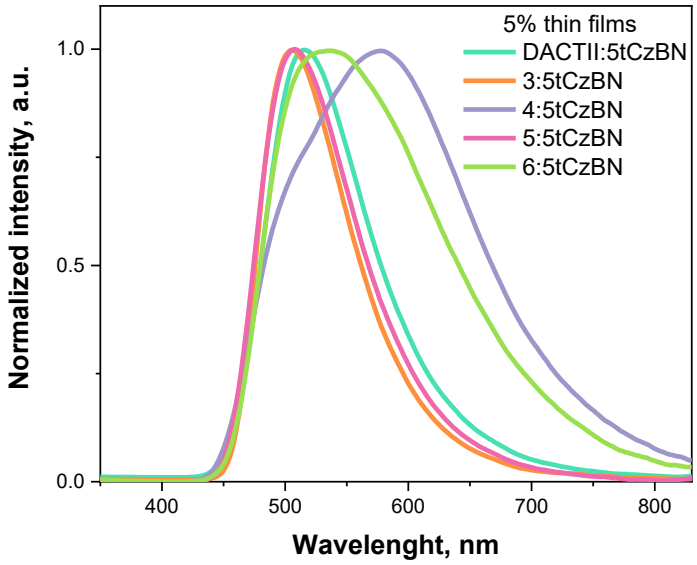

Figure S15. PL spectra of **3-6** and DACT-II 5% wt. in 5tCzBN

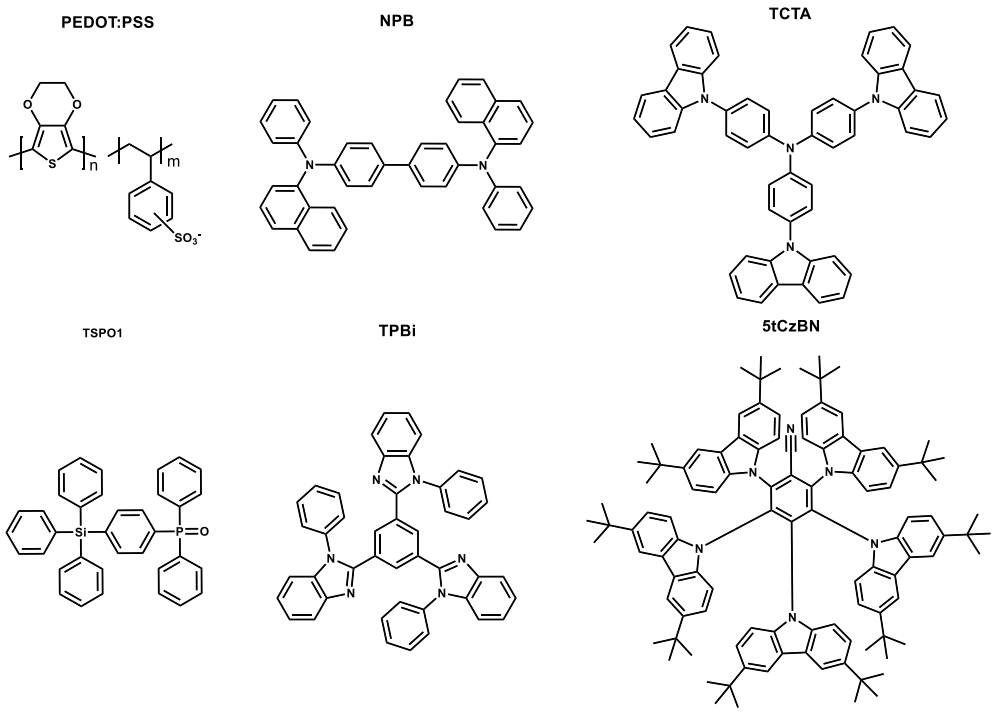

Figure S16. Structures of materials used in the final architecture of OLEDs

Optimisation of OLEDs

At the beginning, we examined host-free and host-containing OLEDs using the following device stack indium-tin-oxide (ITO)/1,4,5,8,9,11-hexaazatriphenyleneheacarbonitrile (HAT-CN) [5 nm]/*N*,*N*'-di(1-naphthyl)-*N,N'*-diphenyl-(1,10-biphenyl)-4,40-diamine (NPB) [50 nm]/emissive layer (EML) [30 nm]/2,2',2''-(1,3,5-benzinetriyl)-tris(1-phenyl-1-H-benzimidazole) (TPBi) [40 nm]/LiF [2 nm]/Al (Figure S17 a). It is marked in these energy diagrams that devices A-D contain the host-free light-emitting layers of **3-6**, respectively. We also fabricated two reference host-free devices, R1 and R2, using commercial green emitters 9-[4-(4,6-diphenyl-1,3,5-triazin-2-yl) phenyl]-N3, N3, N6, N6-tetraphenyl-9H-carbazole-3,6-diamine (DACT-II)[4] and 1,2,3,5-tetrakis(carbazol-9-yl)-4,6-dicyanobenzene (4CzIPN)[5], respectively. In addition, devices E-H contain light-emitting layers of **3-6** (10 wt%) dispersed in a host 2,3,4,5,6-pentakis(3,6-di-*tert*-butyl-9*H*-carbazol-9-yl)benzonitrile (5TCzBN)[6]. In addition, the reference host-containing device R3 was fabricated using commercial orange emitter 2,4,5,6-tetrakis(3,6-diphenylcarbazol-9-yl)-1,3-dicyanobenzene. We should note that the commercial blue TADF emitter 2,3,4,5,6-pentakis(3,6-di-*tert*-butyl-9*H*-carbazol-9-yl)benzonitrile (5TCzBN) was first used as the host in this study (Figure S17 d). There are several reasons why 5TCzBN can be used as the host for

emitters **3-6.** Firstly, the PL spectrum of 5TCzBN overlaps well with the absorption spectra of compounds **3-6**, indicating efficient Förster resonance energy transfer through host–guest interaction (Figure S15). Secondly, HOMO/LUMO levels of compounds **3-6** fall in the energy gap between HOMO-LUMO levels of 5TCzBN. The triplet level, thermal and film-forming properties of 5TCzBN are beneficial for its applications as a host.

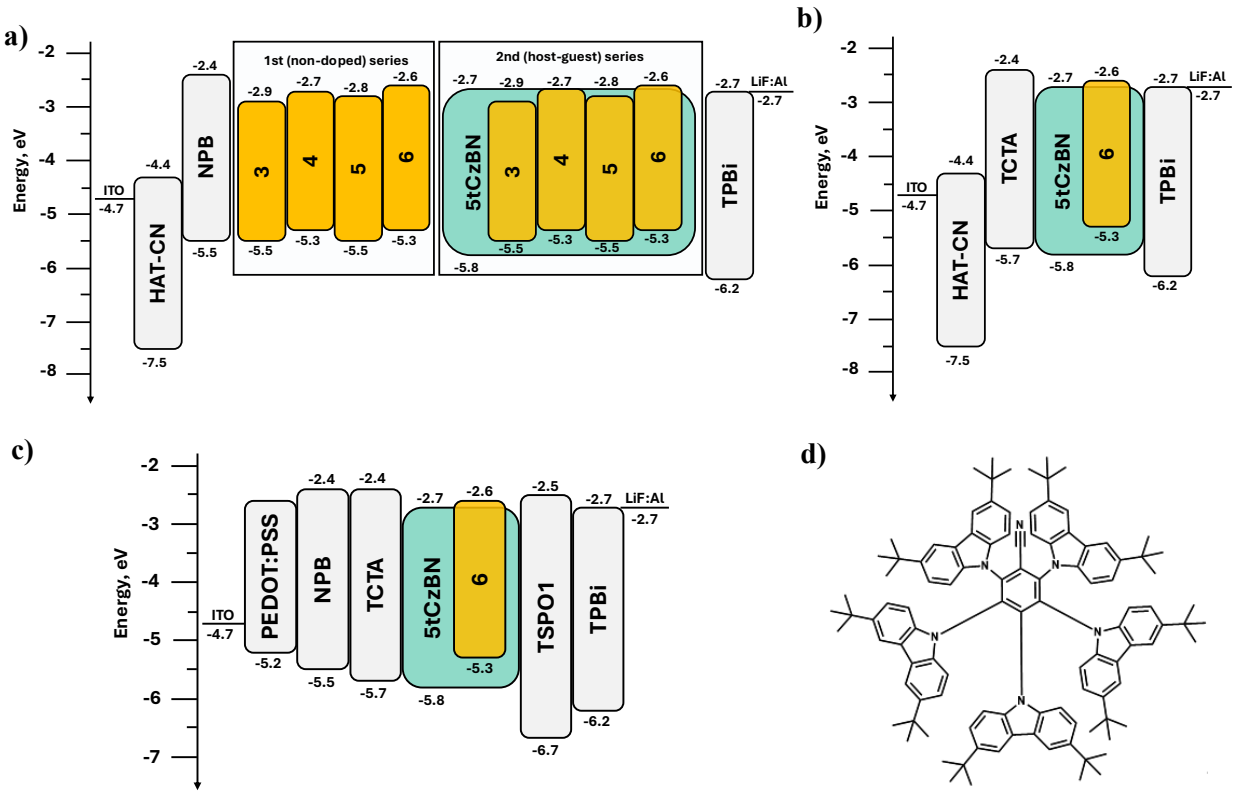

Figure S17. Equilibrium energy diagrams of devices A-H, R1-R3 (a), H1-H4 and R4 (b) and of device H5 (c). Molecular structure of TADF host 5TCzBN (d).

The host free devices A-D showed orange–red electroluminescence. As expected, the EL spectrum of device A is similar to that of C. The EL spectra of OLEDs device B and D are also similar. They peak practically at the same wavelength (see Figure S18 a, Table S1). The EL spectra of devices B and D closely match the PL spectra of the films of **4** and **6**. Meanwhile the EL spectra of devices A and C are visibly red shifted (from green to orange region) with respect to the PL spectra of the films of **3** and **5**. A 1931 Commission Internationale de l'éclairage (CIE) diagram is plotted in Figure S16 b, with the corresponding CIE *x* and *y* coordinates provided in the top right corner.

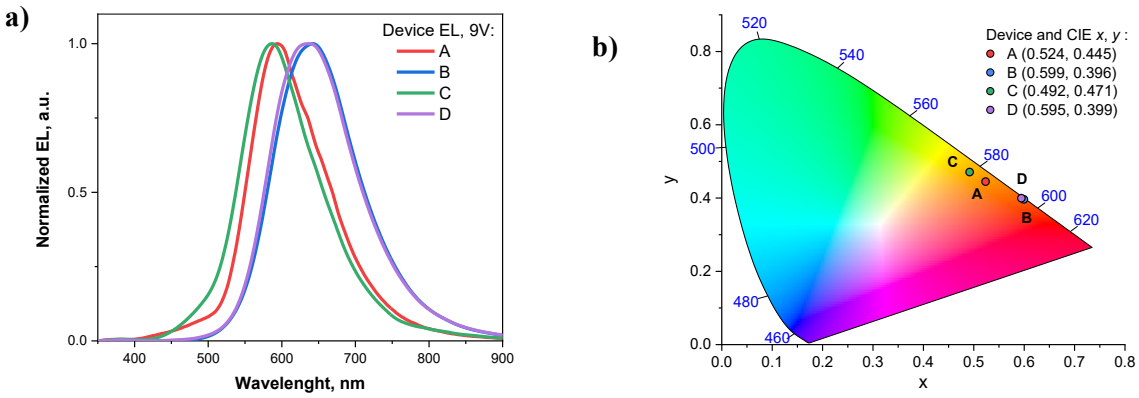

Figure S18. EL spectra (a) and CIE plot (b) of devices A-D.

The EQE of devices A–D fall within the range of 0.34–0.94% (see Table S1). Device B showed the best performance (0.94%). The reference devices, R1 (with DACT-II) showed considerably higher EQE of 6.62% (Table S1). However, the characteristics of the devices are not directly comparable, as R1 showed green electroluminescence peaking at 536 nm, while OLEDs A-D exhibited orange-red EL in the range of 584–643 nm. It is generally known that green devices tend to outperform red ones[7]. Therefore, a more appropriate benchmark would be the device R2 (with 4CzIPN), which emits at the similar wavelengths as OLEDs A–D. In this context, devices A–D outperform R2 (EQE = 0.18%). The low efficiencies observed for host-free devices are consistent with the low PLQY of the neat thin films, as discussed previously, suggesting that insufficient suppression of non-radiative decay and intermolecular interactions limits device performance.

The EL spectra of host-containing devices E-H experienced hypsochromic (blue) shifts compared to those of the host-free devices (A-D). OLEDs E-H exhibited electroluminescence in the range of 495–587 nm (see Table S2, Figure S19 a). The turn-on voltages of the devices ranged from 5.1 to 5.5 V at 10 cd/m^2 (Table S2). The EQE ranged from 0.65 to 8.5%, with the current efficiency (CE) range of 1.7 – 19.7 cd/A and a power efficiency (PE) ranging from 0.9 to 13.3 lm/W (Table S2). Device H was found to show the best performance in this series (EQE of 8.5%, CE of 19.7 cd/A and PE of 13.3 lm/w). It showed comparable, although slightly worse results than the reference OLED R3 (EQE of 9.3%, CE of 29.5 cd/A and PE of 14.5 lm/W). The electroluminescence spectra, CIE color space diagram, the plots of brightness and current density versus voltage (JVL) and EQE versus current density curves are presented in Figure S19.

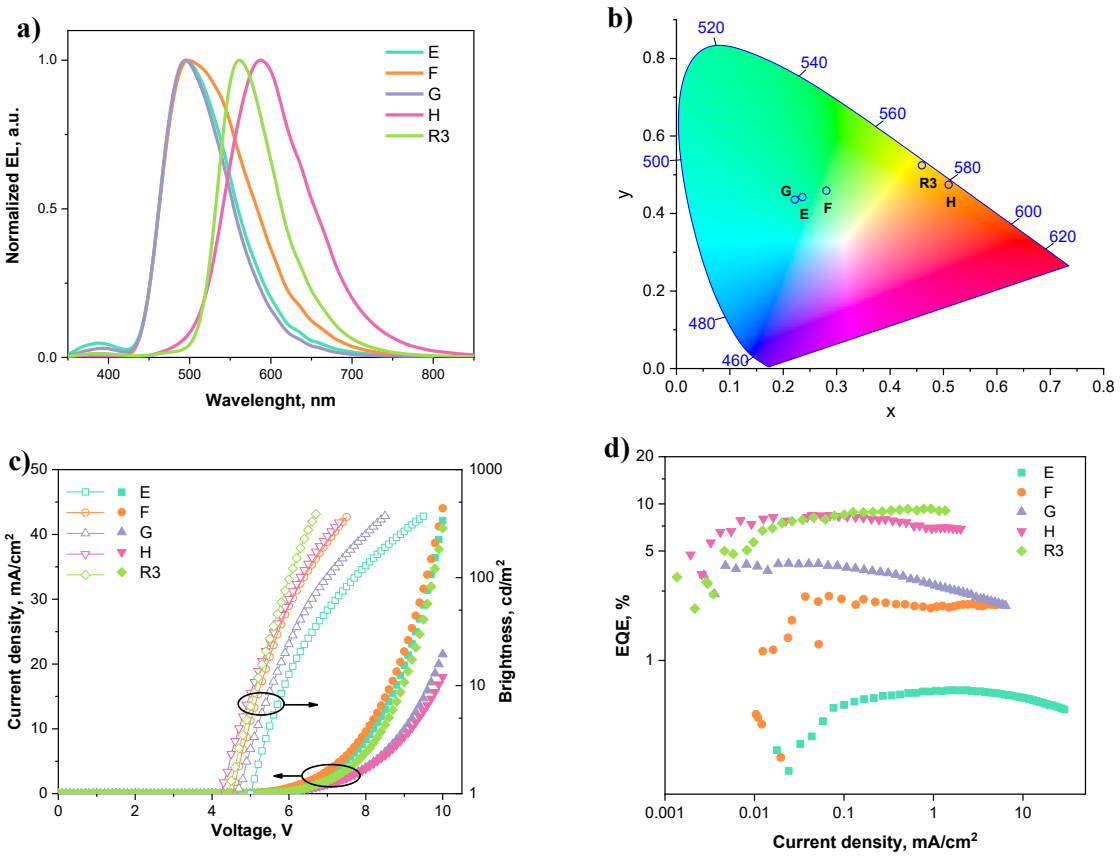

Figure S19. Electro-optical properties of devices E-H and R3. (a) EL spectra of OLEDs; (b) CIE diagram (*x*, *y* coordinates provided in Table 4); (c) plots of brightness and current density versus voltage (JVL); (d) plots of EQE versus current density.

It was decided to further optimize the **6** based device since it showed the most promising results. The stacks of OLED H1-H4 remained the same, however NPB was replaced by 4,4',4"-tris(carbazol-9-yl)triphenylamine (TCTA) (Figure S17 b).

Tables

Table S1. Output electroluminescent parameters of host-free devices A-D, R1, and R2.

Device	Emitter	Host	λ[a], nm	V_{on}[b], V	Max Brightness, cd/m^2	CE[c], cd/A	PE[c], lm/W	EQE[c], %
A	**3**	-	590	3.7	1160	1.29	0.86	0.68
B	**4**	-	643	3.5	1420	0.96	0.79	0.94
C	**5**	-	584	4.3	1940	0.75	0.41	0.34
D	**6**	-	635	3.4	1550	0.86	0.70	0.79
R1	**DACT-II**	-	536	2.7	1487	22.9	20.8	6.62
R2	**4CzIPN**	-	607	5.6	175	0.23	0.1	0.18

[a] The electroluminescence maximum. [b] The turn-on voltage at a brightness of 10 cd/m^2. [c] Current efficiency, power efficiency, external quantum efficiency.

Table S2. Output electroluminescent parameters of host-containing devices E-H, and R3.

Device	Emitter (x wt. %)	Host	λ, nm [a]	CIE, x, y	V_{on}, V [b]	CE, cd/A [c]	PE, lm/W [c]	EQE, % [c]
ITO/HAT-CN/NPB/EML/TPBi/LiF/Al								
E	**3 (10%)**	**5tCzBN**	495	0.222, 0.436	5.2	1.7	0.9	0.65
F	**4 (10%)**		500	0.236, 0.442	5.3	6.9	4.4	2.5
G	**5 (10%)**		495	0.281, 0.459	5.5	10.8	6.9	4.2
H	**6 (10%)**		587	0.510, 0.474	5.1	19.7	13.3	8.5
R3	**4CzIPN-Ph (10%)**		567	0.460, 0.524	5.2	29.5	14.5	9.3

References

1 C. Adamo and V. Barone, *J. Chem. Phys.*, 1999, **110**, 6158–6170.

2 F. Weigend and R. Ahlrichs, *Phys. Chem. Chem. Phys.*, 2005, **7**, 3297–3305.

3 M. J. Frisch, G. W. Trucks, H. B. Schlegel, G. E. Scuseria, M. A. Robb, J. R. Cheeseman, G. Scalmani, V. Barone, G. A. Petersson, H. Nakatsuji, X. Li, M. Caricato, A. V. Marenich, J. Bloino, B. G. Janesko, R. Gomperts, B. Mennucci, H. P. Hratchian, J. V. Ortiz, A. F. Izmaylov, J. L. Sonnenberg, D. Williams-Young, F. Ding, F. Lipparini, F. Egidi, J. Goings, B. Peng, A. Petrone, T. Henderson, D. Ranasinghe, J. Gao, N. Rega, G. Zheng, W. Liang, M. Hada, M. Ehara, K. Toyota, R. Fukuda, J. Hasegawa, M. Ishida, T. Nakajima, Y. Honda, O. Kitao, H. Nakai, T. Vreven, K. Throssell, J. A. Montgomery, J. E. P. Jr., F. Ogliaro, M. J. Bearpark, J. J. Heyd, E. N. Brothers, K. N. Kudin, V. N. Staroverov, T. A. Keith, R. Kobayashi, J. Normand, K. Raghavachari, A. P. Rendell, J. C. Burant, S. S. Iyengar, J. Tomasi, M. Cossi, J. M. Millam, M. Klene, C. Adamo, R. Cammi, J. W. Ochterski, R. L. Martin, K. Morokuma, O. Farkas, J. B. Foresman and D. J. Fox, 2016, preprint.

4 H. Kaji, H. Suzuki, T. Fukushima, K. Shizu, K. Suzuki, S. Kubo, T. Komino, H. Oiwa, F. Suzuki, A. Wakamiya, Y. Murata and C. Adachi, *Nat. Commun.,* 2015, **6**, 8476.

5 H. Uoyama, K. Goushi, K. Shizu, H. Nomura and C. Adachi, *Nature*, 2012, **492**, 234–238.

6 D. Zhang, M. Cai, Y. Zhang, D. Zhang and L. Duan, *Mater. Horiz.*, 2016, **3**, 145–151.

7 H. Shi, W. Jing, W. Liu, Y. Li, Z. Li, B. Qiao, S. Zhao, Z. Xu and D. Song, *ACS Omega*, 2022, **7**, 7893–7900.